(41). Primer and siRNA sequences are listed in supplemental Tables 1 and 2, respectively.

Immunoprecipitation Assay and Western Blotting—For the immunoprecipitation assay, cells were lysed in buffer A (20 mM Tris-HCl (pH 7.5), 50 mM NaCl, 2.5 mM EDTA, 0.5% Nonidet P-40, 1 mM DTT, 0.1 mM PMSF, 2 μg/ml aprotinin, 2 μg/ml leupeptin, and 1 μg/ml RNase A (Sigma)) at 4 °C for 30 min. The mixture was centrifuged at 15,000 × *g* for 20 min, and the supernatant was subsequently incubated with anti-FLAG-agarose (Sigma) at 4 °C for 1 h. The resin was then washed three times with buffer A. Bound protein was eluted with SDS-PAGE sample buffer and analyzed by Western blotting. For analysis of the total cell lysate by Western blotting, cells were harvested and then boiled with SDS-PAGE sample buffer. Antibodies for Western blotting were as follows: anti-FLAG (Sigma), anti-Myc (Roche Applied Science), anti-GST (Cell Signaling), anti-Hbs1 (raised against His-tagged Hbs1), anti-Dom34 (raised against His-tagged Dom34), anti-GAPDH (Millipore or raised against His-tagged GAPDH), anti-Ski2 (Proteintech), and anti-Dis3 (Santa Cruz Biotechnology).

RESULTS

Both Non-stop mRNA and Protein Are Expressed at Lower Levels in Mammalian Cells—To analyze the expression of the gene that lacks a termination codon, we constructed N-terminally FLAG-tagged β-globin reporter genes: FLAG-β-globin control (FBG control) and FLAG-β-globin non-stop (FBG non-stop). The FBG control reporter was generated by mutating two in-frame termination codons in the 3′-UTR of the FLAG-β-globin reporter (21). The FBG non-stop reporter was generated by removing the *bona fide* termination codon of FBG control. Furthermore, we constructed 5×FLAG-tagged β-globin reporter genes: 5×FLAG-β-globin control (5FBG control) and 5×FLAG-β-globin non-stop (5FBG non-stop) (Fig. 1*A*) because FLAG-β-globin proteins were not detectable by Western blotting using anti-FLAG antibody.

We first examined the amount of mRNA and protein produced from the reporter genes at steady state. HeLa cells were cotransfected with either p5FBG control or p5FBG non-stop and a reference plasmid expressing EGFP as a transfection/loading control. Western blot analysis of the total cell lysate showed that 5FBG non-stop protein was decreased to 8 ± 2% of the control (Fig. 1*B*, compare *lanes 6* and *7*). 5FBG non-stop migrated on the SDS-polyacrylamide gel at 30~40 kDa (Fig. 1*B*, *lane 7*) because polylysine is translated from the poly(A) tail of the mRNA to cause ribosome stalling on the poly(A) tail (42). In contrast, Northern blot analysis of total cellular RNA showed that the steady-state level of 5FBG non-stop mRNA was decreased to 48 ± 6% of the control (Fig. 1*C*, *lane 2*). Thus, 5FBG non-stop protein and mRNA were both expressed at a lower level.

It has been shown that non-stop mRNAs are degraded via a Ski7-dependent pathway in yeast (23, 22, 43). In mammals, Hbs1 is most closely related to Ski7 and is established as a regulator of no-go decay. Also, a previous study demonstrated that a single gene referred to as *HBS1/SKI7* from *Lachancea kluyveri* can complement both *ski7*Δ and *hbs1*Δ mutants of *Saccharomyces cerevisiae* (44). This led us to speculate that human Hbs1 might be involved in the decay of non-stop mRNA. Thus, we adopted a siRNA-mediated knockdown strategy to assess the effect of Hbs1 knockdown on the expression of non-stop mRNA and protein. Western blot analysis showed that both Hbs1 siRNA-1 and Hbs1 siRNA-2 efficiently reduced cellular Hbs1 protein (Fig. 1*D*). The down-regulation of Hbs1 expression increased the level of 5FBG non-stop mRNA (Fig. 1*C*, compare *lanes 2* and *3*) and protein (Fig. 1*B*, compare *lanes 7–9*). We conclude that Hbs1 functions in the reduction of non-stop mRNA in mammalian cells. Hbs1 in mammals is suggested to play the same role in non-stop mRNA decay as Ski7 in yeast.

Knockdown of Hbs1 increased the amount of 5FBG non-stop mRNA to a level comparable to 5FBG control mRNA (94 ± 15%) (Fig. 1*C*, compare *lanes 1* and *3*) but the level of 5FBG non-stop protein to 21 ± 3% of that of 5FBG control protein (Fig. 1*B*, compare *lanes 6*, *8*, and *9*). Based on previous studies, the difference seemed to be caused by selective degradation of 5FBG non-stop protein and/or translational repression of 5FBG non-stop (36, 42, 45, 46). It has been shown that Ltn1-mediated ubiquitination of non-stop proteins results in their degradation in yeast (45, 46). Ltn1 is conserved among eukaryotes, and its mammalian ortholog is known as listerin (47). Therefore, we next assessed whether the mechanism of non-stop protein degradation by the E3 ubiquitin ligase is functional in mammalian cells. We examined the effect of siRNA-mediated knockdown of listerin on the reduced expression of non-stop mRNA and protein. Real-time PCR analysis showed that listerin siRNA-1 and listerin siRNA-2 down-regulated listerin mRNA expression to 26 ± 12 and 30 ± 12% of the control level, respectively (Fig. 1*E*). The down-regulation increased the level of 5FBG non-stop protein to 68 ± 14 and 66 ± 2% of that of 5FBG control protein, respectively (Fig. 1*B*, compare *lanes 7*, *10*, and *11*) but had little effect on 5FBG non-stop mRNA (Fig. 1*C*, *lanes 2* and *4*). These results indicate that the expression of non-stop mRNA is reduced not only at the mRNA level but also at the protein level, and the latter is mostly mediated by the listerin E3 ubiquitin ligase.

Decay of Unstable Non-stop mRNA Requires Translation—To gain a better understanding of the decay pathways of non-stop mRNA in mammalian cells, we next analyzed the decay kinetics. For this purpose, we used the FBG reporter instead of the 5FBG reporter because FBG mRNA migrated faster than 5FBG on agarose gel and was separated clearly from 5×FLAG-EGFP mRNA (transfection/loading control). The steady-state level of FBG non-stop mRNA was decreased to 51 ± 11% of FBG control mRNA (Fig. 2*A*, *lane 2*), which is similar to the result using 5FBG reporter constructs (Fig. 1*C*, *lane 2*).

To determine whether the reduced expression of non-stop mRNA was due to increased decay of the mRNA, the decay kinetics of the non-stop mRNA was monitored using a tetracycline regulatory transcriptional pulse-chase approach as described previously (21, 41). HeLa cells were transfected with a transcriptional repressor plasmid expressing the tetracycline receptor, a reference plasmid expressing 5×FLAG-EGFP, and either the FBG control (Fig. 2*B*, *lanes 1–5*) or FBG non-stop (*lanes 6–10*) reporter plasmid. The half-lives of FBG control and FBG non-stop mRNAs were 17.5 ± 4.8 and 6.1 ± 0.8 h,

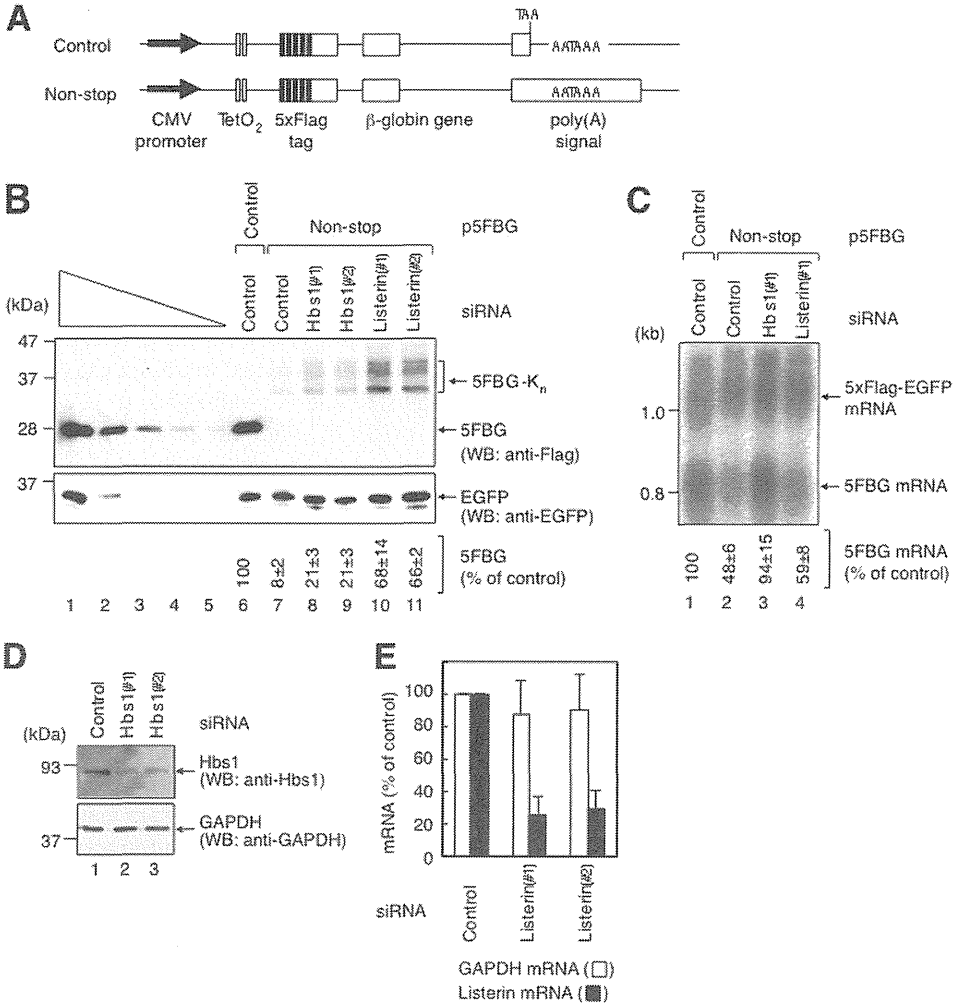

FIGURE 1. **Both non-stop mRNA and protein are expressed at lower levels in HeLa cells.** *A*, diagram of each of the two 5×FLAG-β-globin constructs. *Arrows* indicate the CMV promoter. *Open boxes* indicate the coding frame. *Black boxes* indicate the FLAG tag. Gray boxes indicate the tetracycline operator ($TetO_2$). *B*, listerin functions in the reduced expression of non-stop protein. HeLa cells were transfected with pEGFP-C1; either p5FBG control (*lanes 1–6*) or p5FBG non-stop (*lanes 7–11*); and control luciferase siRNA (*lanes 6* and *7*), Hbs1 siRNA-1 (*Hbs1(#1); lane 8*), Hbs1 siRNA-2 (*Hbs1(#2); lane 9*), listerin siRNA-1 (*Listerin(#1); lane 10*), or listerin siRNA-2 (*Listerin(#2); lane 11*). Total cell lysate was analyzed by Western blotting (*WB*) using anti-FLAG (*upper panel*) or anti-EGFP (*lower panel*) antibody. *Lanes 1–5*, in which 3-fold dilutions of the lysate were analyzed, show that the condition is semiquantitative. *Numbers* immediately below each lane represent the level of 5×FLAG-β-globin protein normalized to the level of EGFP protein, with the level calculated from *lane 1* defined as 100%. *C*, Hbs1 functions in the reduced expression of non-stop mRNA. HeLa cells were transfected with p5×FLAG-EGFP; either p5FBG control (*lane 1*) or p5FBG non-stop (*lanes 2–4*); and control luciferase siRNA (*lanes 1* and *2*), Hbs1 siRNA-1 (*lane 3*), or listerin siRNA-1 (*lane 4*). *Numbers* immediately below each lane represent the level of 5FBG mRNA normalized to the level of 5×FLAG-EGFP mRNA. *D*, down-regulation of Hbs1 expression. HeLa cells were transfected with control luciferase siRNA (*lane 1*), Hbs1 siRNA-1 (*lane 2*), or Hbs1 siRNA-2 (*lane 3*). Total cell lysate was analyzed by Western blotting using anti-Hbs1 (*upper panel*) or anti-GAPDH (*lower panel*) antibody. *E*, down-regulation of listerin expression. HeLa cells were transfected with control luciferase siRNA, listerin siRNA-1, or listerin siRNA-2. Total RNA isolated from the cells was analyzed by real-time PCR. The levels of listerin and GAPDH mRNAs were quantitated. Results in *B–E* are representative of three independently performed experiments.

respectively (Fig. 2*B*, *lower panel*). We conclude that non-stop mRNA is degraded fast in HeLa cells.

Non-stop mRNA decay is characterized by its dependence on translation in yeast (23, 43). To confirm that the decay observed for non-stop mRNA in mammalian cells meets this criteria, we first analyzed the effect of cycloheximide on the mRNA decay. Cycloheximide treatment greatly increased the half-life of FBG non-stop mRNA from 5.7 ± 0.9 h to >18 h (Fig. 2*C*, compare *lanes 1–5* and *6–10*). These results are consistent with previous reports showing that a translation inhibitor increases the level of non-stop mRNA at steady state (23, 37). To further confirm the translation dependence, we constructed an FBG non-stop reporter bearing an IRE within its 5′-UTR (48, 49) and analyzed the mRNA decay of IRE-FBG non-stop mRNA. When hemin was added as an iron source to inactivate iron regulatory protein and permit translation, the half-life of IRE-FBG non-stop mRNA was decreased from 22.6 ± 5.9 to 7.5 ± 1.4 h (Fig. 2*C*, compare *lanes 11–15* and *16–20*). We conclude that translation is required for the fast decay of non-stop mRNA.

Non-stop mRNA Decay Requires Hbs1 and Dom34—As described above, Hbs1 is involved in the reduction of non-stop mRNA in mammalian cells (Fig. 1*C*). To determine whether Hbs1 functions in the fast degradation of non-stop mRNA, we applied a knockdown approach to the transcriptional pulse-chase analysis. HeLa cells were transfected with either Hbs1 siRNA-1 (Fig. 3*B*, *lane 11*-20) or control siRNA (*lanes 1–10*) and a transcriptional repressor plasmid expressing the tetracy-

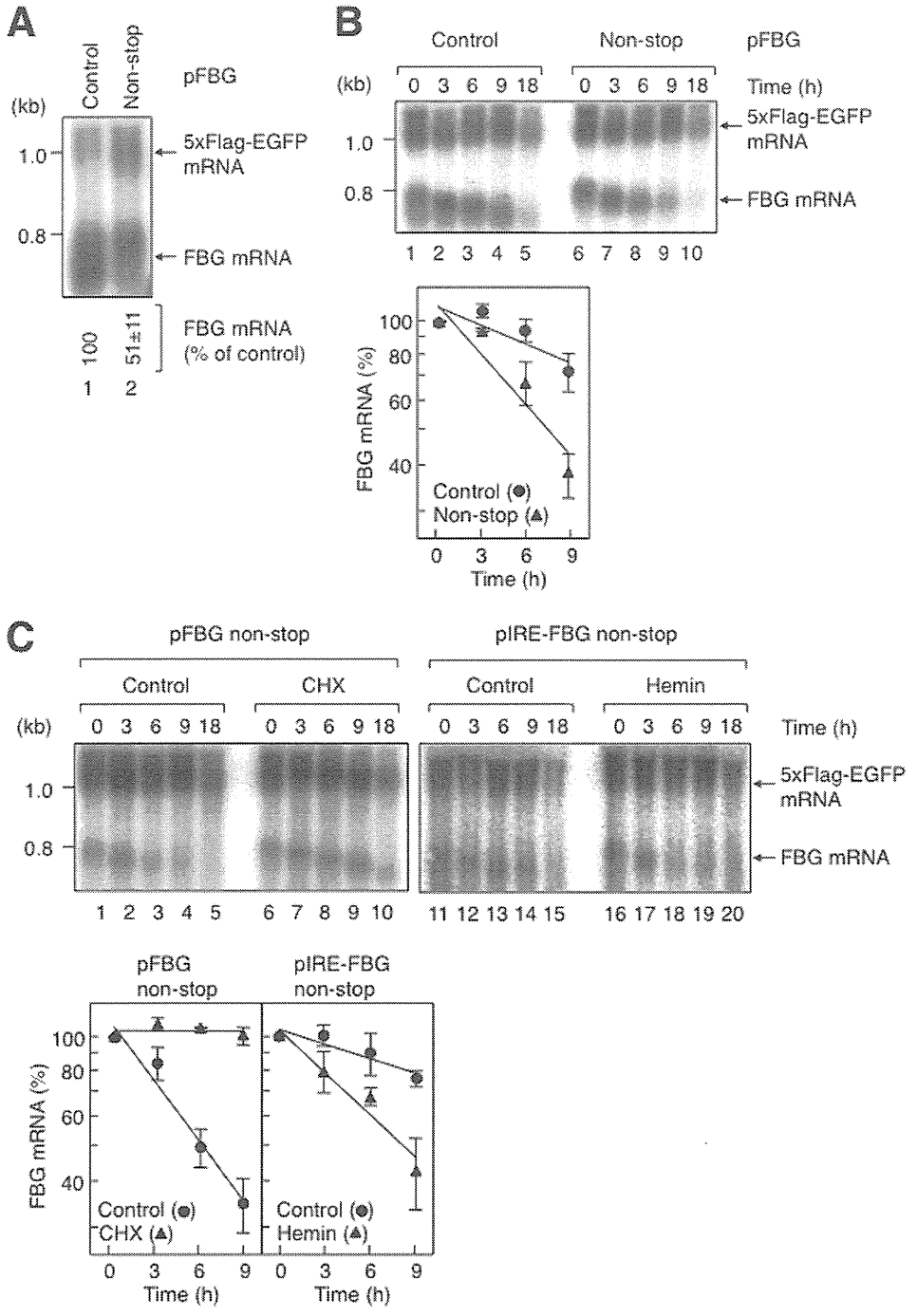

FIGURE 2. **Non-stop mRNA is unstable, and its decay requires translation in HeLa cells.** *A*, steady-state levels of β-globin non-stop mRNAs. HeLa cells were transfected with p5×FLAG-EGFP and either pFBG control (*lane 1*) or pFBG non-stop (*lane 2*). *Numbers* immediately below each lane represent the level of FBG mRNA normalized to the level of 5×FLAG-EGFP mRNA. *B*, degradation of β-globin non-stop mRNAs. HeLa cells were cotransfected with p5×FLAG-EGFP, pT7-TR, and either pFBG control (*upper panel*, *lanes 1–5*) or pFBG non-stop (*lanes 6–10*). 1 day later, FBG mRNA expression was induced by tetracycline for 2.5 h, and the cells were harvested at the specified times after stopping FLAG-β-globin mRNA transcription. The levels of wild-type FBG mRNAs, which were normalized to the levels of 5×FLAG-EGFP mRNAs, were quantitated with the levels of the mRNA from the 0-h time point defined as 100% (*lower panel*). *C*, translation is required for the fast degradation of β-globin non-stop mRNA. HeLa cells were cotransfected with p5×FLAG-EGFP, pT7-TR, and either pFBG non-stop (*upper panel*, *lanes 1–10*) or pIRE-FBG non-stop (*lanes 11–20*). The transcriptional pulse-chase analysis was performed as described for *B*, except that the cells were treated with 100 μg/ml cycloheximide (*CHX*; *upper panel*, *lanes 6–10*) or 50 μM hemin (*lanes 16–20*). The levels of FBG mRNAs were quantitated as described for *B* (*lower panel*). *Error bars* represent S.D. for three independent experiments.

cline receptor, a reference plasmid expressing 5×FLAG-EGFP, and either the FBG control (Fig. 3*B*, *lanes 1–5* and *11–15*) or FBG non-stop (*lanes 6–10* and *16–20*) reporter plasmid. Down-regulation of Hbs1 protein expression was confirmed by Western blotting using anti-Hbs1 antibody and, as a control, anti-GAPDH antibody (Fig. 3*A*, compare *lanes 1* and *2*). This down-regulation increased the half-life of FBG non-stop mRNA from 5.3 ± 0.9 to 12.9 ± 2.6 h (Fig. 3*B*, compare *lanes 6–10* and *16–20*). The half-life of FBG non-stop mRNA was close to that of FBG control mRNA (Fig. 3, *B*, compare *lanes*

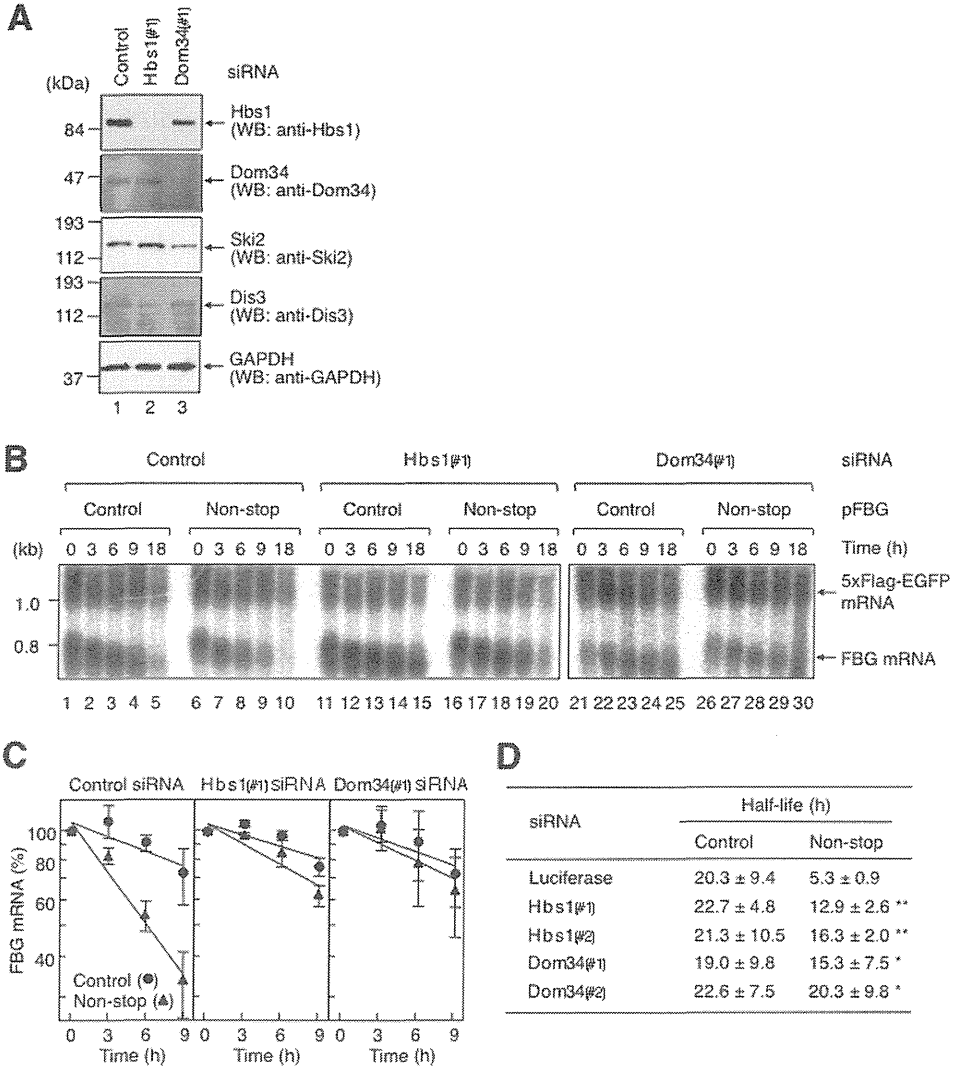

siRNA	Half-life (h)	
	Control	Non-stop
Luciferase	20.3 ± 9.4	5.3 ± 0.9
Hbs1(#1)	22.7 ± 4.8	12.9 ± 2.6 **
Hbs1(#2)	21.3 ± 10.5	16.3 ± 2.0 **
Dom34(#1)	19.0 ± 9.8	15.3 ± 7.5 *
Dom34(#2)	22.6 ± 7.5	20.3 ± 9.8 *

FIGURE 3. **Non-stop mRNA decay requires Hbs1 and Dom34.** *A*, down-regulation of Hbs1 and Dom34 expression. HeLa cells were transfected with control luciferase siRNA (*lane 1*), Hbs1 siRNA-1 (*Hbs1(#1)*; *lane 2*), or Dom34 siRNA-1 (*Dom34(#1)*; *lane 3*). Total cell lysate was analyzed by Western blotting (*WB*) using the indicated antibodies. *B*, down-regulation of either Hbs1 or Dom34 expression inhibits fast degradation of non-stop mRNA. HeLa cells were transfected with p5×FLAG-EGFP; pT7-TR; either pFBG control (*lanes 1–5*, *11–15*, and *21–25*) or pFBG non-stop (*lanes 6–10*, *16–20*, and *26–30*); and control luciferase siRNA (*lanes 1–10*), Hbs1 siRNA-1 (*lanes 11–20*), or Dom34 siRNA-1 (*lanes 21–30*). The transcriptional pulse-chase analysis was performed as described in the legend to Fig. 2, except that the siRNAs were cotransfected. *C*, the levels of FBG mRNAs were quantitated as described in the legend to Fig. 2. *D*, the half-lives of FBG mRNAs were calculated. The *asterisks* denote the levels of statistical significance (Student's *t* test) between luciferase siRNA and either Hbs1 or Dom34 siRNA: *, $p < 0.05$; **, $p < 0.01$.

11–15 and *16–20*; and *C*). The increased half-life of FBG non-stop mRNA was obtained with a second siRNA (Hbs1 siRNA-2) whose target sequence was different from that of Hbs1 siRNA-1 (Fig. 3*D*). We conclude that Hbs1 functions in the decay of non-stop mRNA.

Previous studies demonstrated that Hbs1 binds Dom34 directly to form a complex (4), and the Hbs1-Dom34 complex functions in no-go decay (27, 31). These findings prompted us to investigate whether Dom34 is involved in the fast degradation of non-stop mRNA. Knockdown of Dom34 with Dom34 siRNA-1 in HeLa cells was performed as described above for Hbs1 (Fig. 3*A*, compare *lanes 1* and *3*). The down-regulation of Dom34 expression increased the half-life of FBG non-stop mRNA from 5.3 ± 0.9 h to >18 h (Fig. 3*B*, compare *lanes 6–10* and *26–30*). The half-life of FBG non-stop mRNA was equivalent to that of FBG control mRNA (Fig. 3, *B*, compare *lanes 21–25* and *26–30*; and *C*). The increased half-life of FBG non-stop mRNA was also obtained with a second siRNA (Dom34 siRNA-2) whose target sequence was different from that of Dom34 siRNA-1 (Fig. 3*D*). Thus, the down-regulation inhibits fast degradation of non-stop mRNA. However, it should be noted that when Dom34 was depleted, the expression levels of Hbs1 and Ski2 were decreased to 40~60% of the control (Fig. 3*A*). The decreased levels of these proteins could partially contribute to inhibit the fast degradation because Dom34 depletion completely inhibited the fast decay provided that 40~60% of Hbs1 and Ski2 were still remained. Taken together, these results indicate that both Hbs1 and Dom34 function in the decay of non-stop mRNA.

Non-stop mRNA Decay Requires the Exosome-Ski Complex—In yeast, non-stop mRNAs are degraded mainly in a 3′-to-5′ direction by the exosome (23, 22). Thus, we next aimed to

determine whether non-stop mRNAs in mammalian cells are degraded by the exosome complex. We examined the decay of non-stop mRNA upon Ski2 down-regulation for the following two reasons. First, exosome-mediated 3′-to-5′ degradation of general mRNA requires a Ski complex consisting of the helicase Ski2, Ski3, and Ski8 (25, 50). Second, in yeast, the Ski complex binds Ski7, to which Hbs1 is most closely related in mammals (3, 51). Because two different yeast Ski2 homologs, Ski2 and Mtr4, are present in the human genome, we performed siRNA-mediated knockdown of both Ski2 and Mtr4 in HeLa cells.

HeLa cells were transfected with either Ski2 siRNA-1 or Mtr4 siRNA-1 as described above for Hbs1. Down-regulation of Ski2 and Mtr4 was confirmed by Western blotting and real-time PCR, respectively (Fig. 4, *A* and *B*). Ski2 and Mtr4 down-regulation increased the half-life of FBG non-stop mRNA from 4.4 ± 0.5 to 6.8 ± 0.9 and 10.0 ± 2.4 h, respectively (Fig. 4, *C*, compare *lanes 6–10*, *16–20*, and *26–30*; and *D*). The result shows that siRNA-mediated knockdown of either Ski2 or Mtr4 partially increased the half-lives of FBG non-stop mRNA. Therefore, HeLa cells were transfected with both Ski2 siRNA-1 and Mtr4 siRNA-1 as described above. The simultaneous Ski2/Mtr4 down-regulation increased the half-life of FBG non-stop mRNA from 4.4 ± 0.5 to 13.4 ± 4.0 h (Fig. 4, *E*, compare *lanes 6–10* and *16–20*; and *F*). The half-life of FBG non-stop mRNA was equivalent to that of FBG control mRNA upon Ski2/Mtr4 down-regulation (Fig. 4, *E*, compare *lanes 11–15* and *16–20*; and *F*). The increased half-life of FBG non-stop mRNA was also observed with Ski2 siRNA-2 and Mtr4 siRNA-2 (Fig. 4*H*). The expression levels of Hbs1, Dom34, and the exo/endonuclease Dis3 (see below) were not affected by Ski2/Mtr4 down-regulation (Fig. 4*G*). These results suggest that Ski2 and Mtr4 function redundantly in the fast decay of non-stop mRNA.

In yeast, non-stop mRNA is degraded by Rrp44, which has both exonuclease and endonuclease activities conferred by the PIN domain in the N terminus and the RNase II/R domain in the C terminus (26, 52, 53). Human Dis3 is similar to yeast Rrp44 not only in terms of sequence conservation but also in possessing the two distinct ribonucleolytic activities. Although Dis3 is localized mainly in the nucleus, a significant amount of Dis3 is detected in the cytoplasm. Moreover, human Dis3 can complement a yeast Rrp44 disruption (54). To elucidate whether the 3′-to-5′ exonuclease in the exosome complex promotes the degradation of non-stop mRNA in mammalian cells, we next examined the decay of non-stop mRNA by knocking down Dis3. HeLa cells were transfected with Dis3 siRNA-1 as described above for Hbs1. Down-regulation of Dis3 was confirmed by Western blotting using anti-Dis3 antibody and, as a control, anti-GAPDH antibody (Fig. 5*A*). Under this condition, the expression levels of Hbs1, Dom34, and Ski2 were not affected (Fig. 5*A*). The Dis3 down-regulation increased the half-life of FBG non-stop mRNA from 7.0 ± 1.1 to 14.0 ± 5.3 h (Fig. 5*B*, compare *lanes 6–10* and *16–20*; and *C* and *D*). The increased half-life of FBG non-stop mRNA was observed with a second siRNA (Dis3 siRNA-2) whose target sequence was different from that of Dis3 siRNA-1 (Fig. 5*D*). These results indicate that 3′-to-5′ exonuclease in the exosome complex promotes the degradation of non-stop mRNA. Notably, Dis3 is suggested to function predominantly in the decay of non-stop mRNA.

Hbs1-Dom34 Binds to Form a Complex with the Exosome—Ski7 recruits the exosome to non-stop mRNA in yeast (22, 23). If, as in the case of yeast Ski7, Hbs1 functions in the fast degradation of non-stop mRNA in mammalian cells, Hbs1 should interact with the exosome complex. To test this hypothesis, we assessed the interaction between Hbs1 and the exosome complex by conducting co-immunoprecipitation experiments using HeLa cells. HeLa cells were transfected with p5×Myc-Ski2, pMyc-GST, and either pFLAG-Hbs1 or pFLAG, and the cell extract was immunoprecipitated using anti-FLAG antibody. Western blot analysis showed that FLAG-Hbs1 co-purified with 5×Myc-Ski2 (Fig. 6*A*, *lane 5*). When the same experiment was performed with p5×Myc-Dis3 instead of p5×Myc-Ski2, FLAG-Hbs1 also co-purified with 5×Myc-Dis3 (Fig. 6*B*, *lane 5*). Additionally, Myc-GST was not detectably co-purified with FLAG-Hbs1, indicating that 5×Myc-Ski2 and 5×Myc-Dis3 were co-purified specifically (Fig. 6, *A* and *B*, *lower panel*). The interactions seem not to be mediated by RNA because all of these experiments were performed in the presence of RNase A. From these results, we conclude that Hbs1 interacts with the exosome-Ski complex.

As described previously, Hbs1 and Dom34 bind directly, and the formation of the Hbs1-Dom34 complex results in a significant conformational change in Dom34, which increases the affinity of the complex for the A site of the ribosome (32, 55, 56). Thus, in the no-go decay mechanism, Hbs1 and Dom34 are thought to form a complex at the A site of the stalled ribosome. These results led us to speculate that Hbs1 in complex with Dom34 recruits the exosome to the ribosome stalled on non-stop mRNA. To investigate this possibility, we analyzed the interaction between Dom34 and the exosome by conducting co-immunoprecipitation experiments. HeLa cells were cotransfected with pFLAG-Dom34, pMyc-GST, and either p5×Myc-Ski2 (Fig. 6*A*) or p5×Myc-Dis3 (Fig. 6*B*), and the cell extract was immunoprecipitated using anti-FLAG antibody. Western blot analysis showed that both 5×Myc-Ski2 and 5×Myc-Dis3, but not Myc-GST, were co-purified with FLAG-Dom34 (Fig. 6, *A* and *B*, *lane 6*). We conclude that Dom34, as well as Hbs1, interacts with the exosome complex. These results suggest that the exosome is recruited to the Hbs1-Dom34 complex, which is fitted into the stalled ribosome on non-stop mRNA.

DISCUSSION

The presence of a quality control mechanism for aberrant mRNAs lacking in-frame termination codons remained enigmatic in mammalian cells. One of the primary reasons for this is the absence of a Ski7 protein in mammalian cells. Also, it was reported that the decay rate of non-stop mRNA is not different from that of wild-type mRNA (36, 39). In this study, we have demonstrated that a quality control mechanism for aberrant non-stop mRNA actually exists in mammalian cells based on the following five criteria. (i) Non-stop mRNA is unstable and degraded quickly (Fig. 2*B*); (ii) the decay is dependent on translation (Fig. 2*C*); (iii) the decay requires an eRF3 family GTP-binding protein (Fig. 3); (iv) the decay requires the exosome-Ski

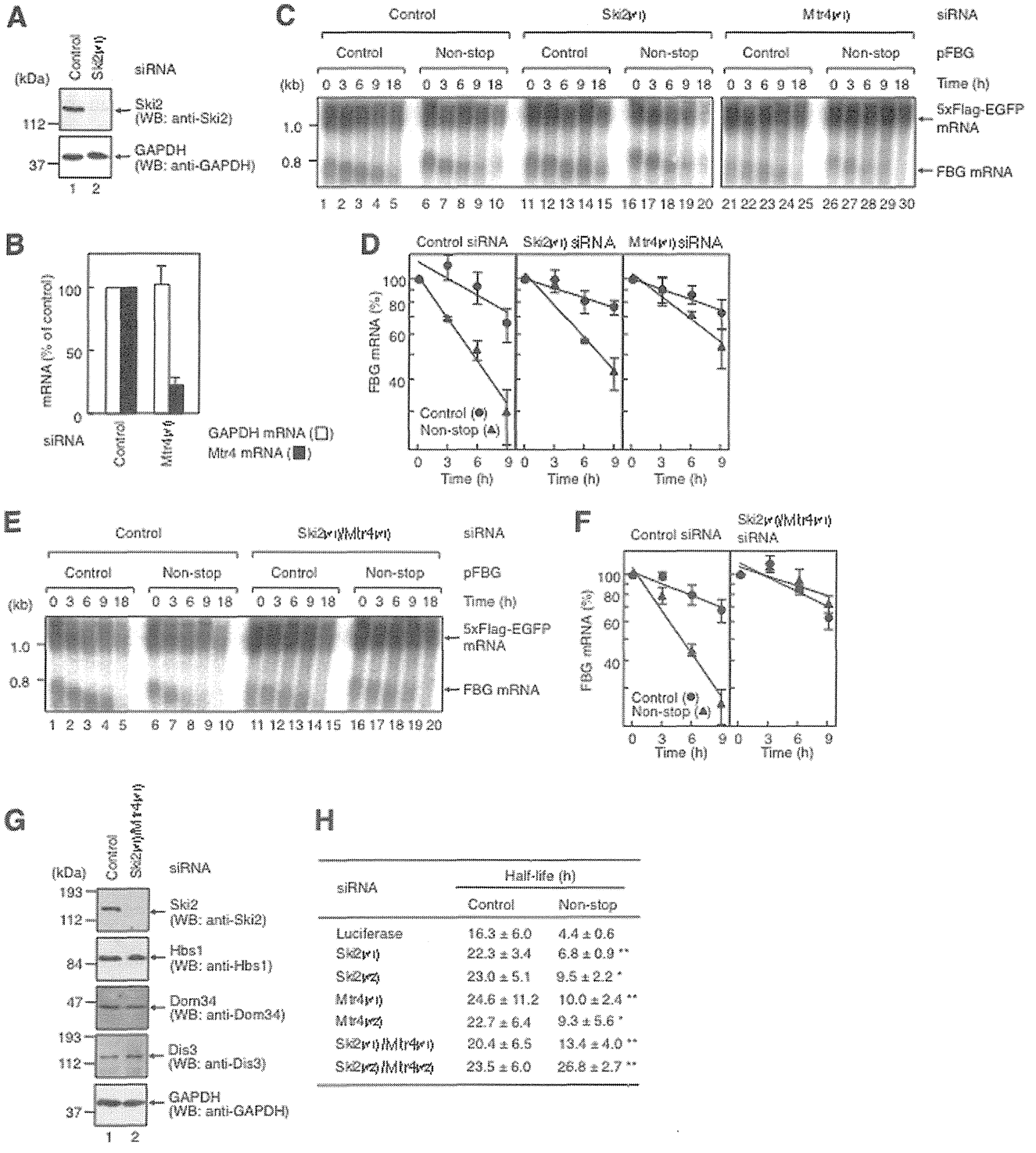

H

siRNA	Half-life (h)	
	Control	Non-stop
Luciferase	16.3 ± 6.0	4.4 ± 0.6
Ski2(#1)	22.3 ± 3.4	6.8 ± 0.9 **
Ski2(#2)	23.0 ± 5.1	9.5 ± 2.2 *
Mtr4(#1)	24.6 ± 11.2	10.0 ± 2.4 **
Mtr4(#2)	22.7 ± 6.4	9.3 ± 5.6 *
Ski2(#1)/Mtr4(#1)	20.4 ± 6.5	13.4 ± 4.0 **
Ski2(#2)/Mtr4(#2)	23.5 ± 6.0	26.8 ± 2.7 **

FIGURE 4. **Non-stop mRNA decay requires the exosome-Ski complex.** *A*, down-regulation of Ski2 expression. HeLa cells were transfected with either control luciferase siRNA (*lane 1*) or Ski2 siRNA-1 (*Ski2(#1)*; *lane 2*). Total cell lysate was analyzed by Western blotting (*WB*) using the indicated antibodies. *B*, down-regulation of Mtr4 expression. HeLa cells were transfected with control luciferase siRNA or Mtr4 siRNA-1 (*Mtr4(#1)*). Total RNA isolated from the cells was analyzed by real-time PCR. The levels of Mtr4 and GAPDH mRNAs were quantitated. Results are representative of three independently performed experiments. *C*, down-regulation of either Ski2 or Mtr4 expression partially inhibits fast degradation of non-stop mRNA. HeLa cells were transfected with p5×FLAG-EGFP; pT7-TR; either pFBG control (*lanes 1–5*, *11–15*, and *21–25*) or pFBG non-stop (*lanes 6–10*, *16–20*, and *26–30*); and control luciferase siRNA (*lanes 1–10*), Ski2 siRNA-1 (*lanes 11–20*), or Mtr4 siRNA-1 (*lanes 21–30*). The transcriptional pulse-chase analysis was performed as described in the legend to Fig. 3. *D*, the levels of FBG mRNAs were quantitated as described in the legend to Fig. 2. *E*, down-regulation of Ski2/Mtr4 expression inhibits fast degradation of non-stop mRNA. HeLa cells were transfected with p5×FLAG-EGFP, pT7-TR, either pFBG control (*lanes 1–5* and *11–15*) or pFBG non-stop (*lanes 6–10* and *16–20*), and either control luciferase siRNA (*lanes 1–10*) or Ski2 siRNA-1/Mtr4 siRNA-1 (*lanes 11–20*). The transcriptional pulse-chase analysis was performed as described in the legend to Fig. 2, except that the siRNAs were cotransfected. *F*, the levels of FBG mRNAs were quantitated as described in the legend to Fig. 2. *G*, down-regulation of Ski2/Mtr4 expression. HeLa cells were transfected with control luciferase siRNA (*lane 1*) or Ski2 siRNA-1/Mtr4 siRNA-1 (*lane 2*). Total cell lysate was analyzed by Western blotting using the indicated antibodies. *H*, the half-lives of FBG mRNAs were calculated. The *asterisks* denote the levels of statistical significance (Student's *t* test) between luciferase siRNA and either Ski2 or Mtr4 siRNA: *, $p < 0.05$; **, $p < 0.01$.

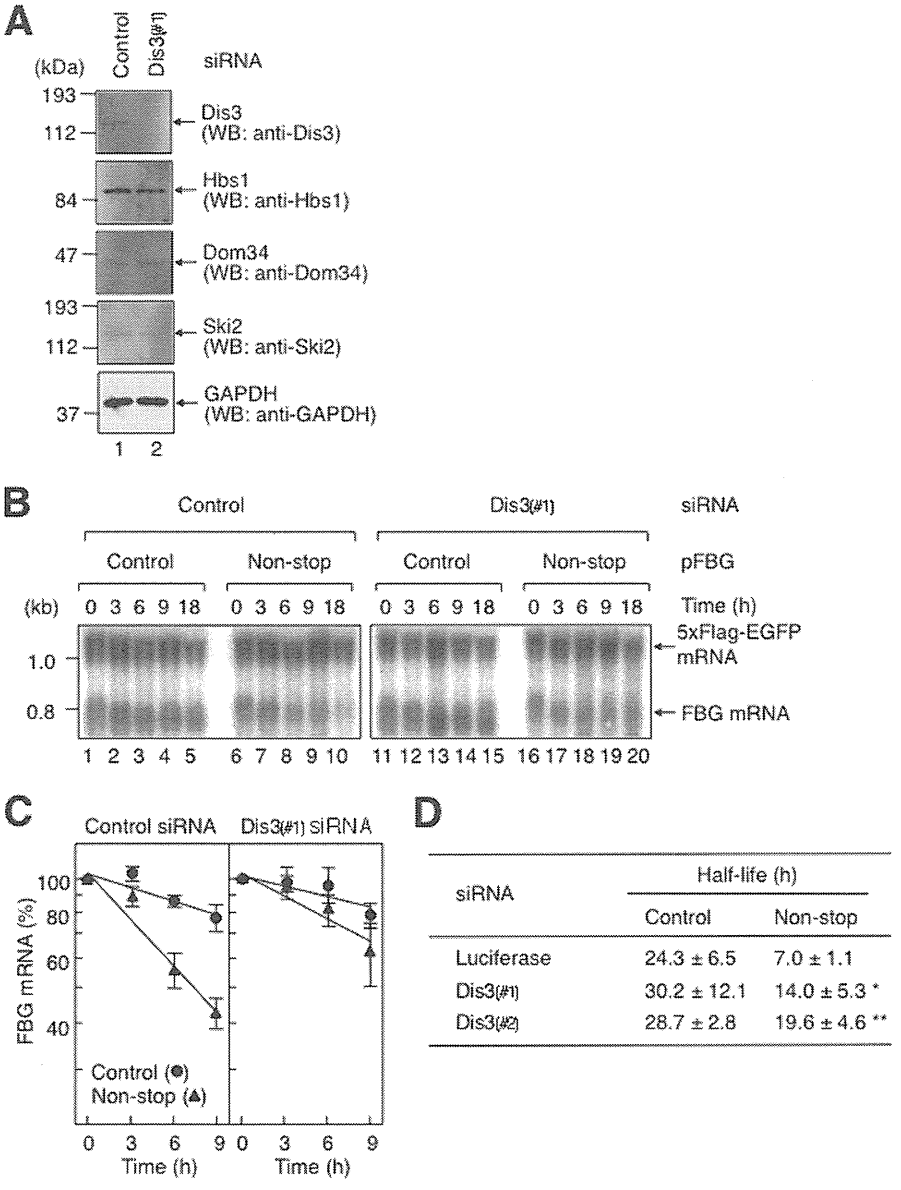

siRNA	Half-life (h)	
	Control	Non-stop
Luciferase	24.3 ± 6.5	7.0 ± 1.1
Dis3(#1)	30.2 ± 12.1	14.0 ± 5.3 *
Dis3(#2)	28.7 ± 2.8	19.6 ± 4.6 **

FIGURE 5. **Non-stop mRNA decay requires Dis3.** *A*, down-regulation of Dis3 expression. HeLa cells were transfected with either control luciferase siRNA (*lane 1*) or Dis3 siRNA-1 (*Dis3(#1); lane 2*). Total cell lysate was analyzed by Western blotting (*WB*) using the indicated antibodies. *B*, down-regulation of Dis3 expression inhibits fast degradation of non-stop mRNA. HeLa cells were transfected with p5×FLAG-EGFP, pT7-TR, either pFBG control (*lanes 1–5* and *11–15*) or pFBG non-stop (*lanes 6–10* and *16–20*), and either control luciferase siRNA (*lanes 1–10*) or Dis3 siRNA-1 (*lanes 11–20*). The transcriptional pulse-chase analysis was performed as described in the legend to Fig. 2. *C*, the levels of FBG mRNAs were quantitated as described in the legend to Fig. 2. *D*, the half-lives of FBG mRNAs were calculated. The *asterisks* denote the levels of statistical significance (Student's *t* test) between luciferase and Dis3 siRNAs: *, $p < 0.05$;**, $p < 0.01$.

complex (Figs. 4 and 5); and (v) the decay-regulating eRF3 family G protein forms a complex with the exosome (Fig. 6).

Thus, as in yeast, an eRF3-like GTP-binding protein, the exosome, and a Ski complex are all involved in the decay of non-stop mRNA in mammalian cells. This makes it possible to surmise that the Hbs1-Dom34 complex binds to the stalled ribosome at the 3′-end of mRNA and recruits the exosome-Ski complex to degrade the aberrant massage. A major difference is that Hbs1 is used instead of Ski7 in mammalian cells.

Recent findings have demonstrated that Hbs1-Dom34 acts as a ribosome-recycling factor, which dissociates the ribosome into the subunits to release the stalled ribosome from the message (33–35, 57, 58). The findings are reasonable because mRNA with a stalled ribosome is not a good substrate for the 3′-to-5′ exonucleolytic degradation by the exosome. The findings, taken together with our results presented here, suggest that Hbs1-Dom34 binds to the stalled ribosome at the 3′-end of non-stop mRNA and induces both dissociation of the ribosome into the subunits for its recycling and simultaneous recruitment of the exosome-Ski complex for degrading the aberrant message. Very recently, Inada and co-workers (59) also showed that Hbs1 is involved in NSD in the yeast *S. cerevisiae*. However, as described above, saccharomycete yeast cells have a unique member of the eRF3 G protein family, Ski7, which has already been established as a regulator of NSD in yeast. Thus, it is reasonable to assume that in contrast to other organisms, including mammals, saccharomycete yeast cells have evolved a specialized mechanism for NSD, in which two eRF3 family

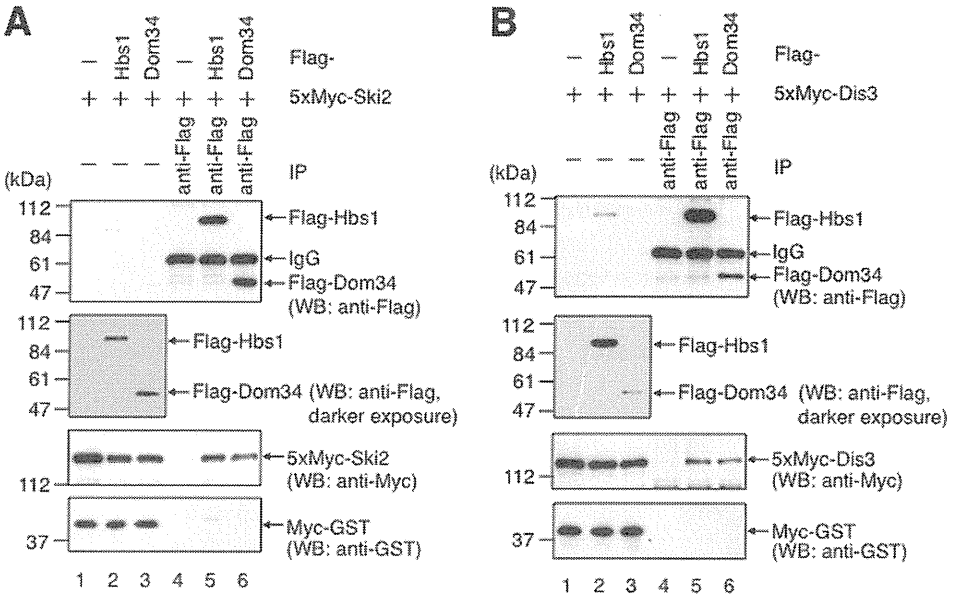

FIGURE 6. **Hbs1 and Dom34 interact with the exosome-Ski complex.** HeLa cells were transfected with either p5×Myc-Ski2 (*A*) or p5×Myc-Dis3 (*B*) and also pFLAG (*lanes 1* and *4*), pFLAG-Hbs1 (*lanes 2* and *5*), or pFLAG-Dom34 (*lanes 3* and *6*). The cell extracts were subjected to an immunoprecipitation (*IP*) assay using anti-FLAG antibody. Immunoprecipitation was performed in the presence of RNase A. The immunoprecipitates (*lanes 4–6*) and inputs (*lanes 1–3*; 10% of the amount immunoprecipitated) were analyzed by Western blotting (*WB*) using the indicated antibodies. The results are representative of three independently performed experiments.

members are involved: the yeast Hbs1 inherited a ribosome-recycling function of the ancestral Hbs1, and Ski7 inherited an exosome-recruiting function.

Also, we have presented data suggesting that the product of non-stop mRNA is subjected to protein quality control and that listerin, the mammalian ortholog of yeast Ltn1, functions as the E3 ubiquitin ligase. More studies are needed to evaluate in detail the mechanisms of the two quality control systems developed for non-stop mRNA and protein.

Acknowledgments—We are grateful to O. Jean-Jean and H. Philippe for providing Hbs1 cDNA.

REFERENCES

1. Hoshino, S., Imai, M., Mizutani, M., Kikuchi, Y., Hanaoka, F., Ui, M., and Katada, T. (1998) Molecular cloning of a novel member of the eukaryotic polypeptide chain-releasing factors (eRF). Its identification as eRF3 interacting with eRF1. *J. Biol. Chem.* **273,** 22254–22259
2. Wallrapp, C., Verrier, S. B., Zhouravleva, G., Philippe, H., Philippe, M., Gress, T. M., and Jean-Jean, O. (1998) The product of the mammalian orthologue of the *Saccharomyces cerevisiae HBS1* gene is phylogenetically related to eukaryotic release factor 3 (eRF3) but does not carry eRF3-like activity. *FEBS Lett.* **440,** 387–392
3. Araki, Y., Takahashi, S., Kobayashi, T., Kajiho, H., Hoshino, S., and Katada, T. (2001) Ski7p G protein interacts with the exosome and the Ski complex for 3′-to-5′ mRNA decay in yeast. *EMBO J.* **20,** 4684–4693
4. Carr-Schmid, A., Pfund, C., Craig, E. A., and Kinzy, T. G. (2002) Novel G-protein complex whose requirement is linked to the translational status of the cell. *Mol. Cell. Biol.* **22,** 2564–2574
5. Frolova, L., Le Goff, X., Rasmussen, H. H., Cheperegin, S., Drugeon, G., Kress, M., Arman, I., Haenni, A. L., Celis, J. E., and Philippe, M. (1994) A highly conserved eukaryotic protein family possessing properties of polypeptide chain release factor. *Nature* **372,** 701–703
6. Stansfield, I., Jones, K. M., Kushnirov, V. V., Dagkesamanskaya, A. R., Poznyakovski, A. I., Paushkin, S. V., Nierras, C. R., Cox, B. S., Ter-Avanesyan, M. D., and Tuite, M. F. (1995) The products of the *SUP45* (eRF1) and *SUP35* genes interact to mediate translation termination in *Saccharomyces cerevisiae*. *EMBO J.* **14,** 4365–4373
7. Zhouravleva, G., Frolova, L., Le Goff, X., Le Guellec, R., Inge-Vechtomov, S., Kisselev, L., and Philippe, M. (1995) Termination of translation in eukaryotes is governed by two interacting polypeptide chain release factors, eRF1 and eRF3. *EMBO J.* **14,** 4065–4072
8. Maquat, L. E. (2004) Nonsense-mediated mRNA decay: splicing, translation and mRNP dynamics. *Nat. Rev. Mol. Cell Biol.* **5,** 89–99
9. Czaplinski, K., Ruiz-Echevarria, M. J., Paushkin, S. V., Han, X., Weng, Y., Perlick, H. A., Dietz, H. C., Ter-Avanesyan, M. D., and Peltz, S. W. (1998) The surveillance complex interacts with the translation release factors to enhance termination and degrade aberrant mRNAs. *Genes Dev.* **12,** 1665–1677
10. Amrani, N., Ganesan, R., Kervestin, S., Mangus, D. A., Ghosh, S., and Jacobson, A. (2004) A faux 3′-UTR promotes aberrant termination and triggers nonsense-mediated mRNA decay. *Nature* **432,** 112–118
11. Nagy, E., and Maquat, L. E. (1998) A rule for termination-codon position within intron-containing genes: when nonsense affects RNA abundance. *Trends Biochem. Sci.* **23,** 198–199
12. Lykke-Andersen, J., Shu, M. D., and Steitz, J. A. (2001) Communication of the position of exon-exon junctions to the mRNA surveillance machinery by the protein RNPS1. *Science* **293,** 1836–1839
13. Kim, V. N., Kataoka, N., and Dreyfuss, G. (2001) Role of the nonsense-mediated decay factor hUpf3 in the splicing-dependent exon-exon junction complex. *Science* **293,** 1832–1836
14. Le Hir, H., Gatfield, D., Izaurralde, E., and Moore, M. J. (2001) The exon-exon junction complex provides a binding platform for factors involved in mRNA export and nonsense-mediated mRNA decay. *EMBO J.* **20,** 4987–4997
15. Kashima, I., Yamashita, A., Izumi, N., Kataoka, N., Morishita, R., Hoshino, S., Ohno, M., Dreyfuss, G., and Ohno, S. (2006) Binding of a novel SMG-1-Upf1-eRF1-eRF3 complex (SURF) to the exon junction complex triggers Upf1 phosphorylation and nonsense-mediated mRNA decay. *Genes Dev.* **20,** 355–367
16. Huntzinger, E., Kashima, I., Fauser, M., Saulière, J., and Izaurralde, E. (2008) SMG6 is the catalytic endonuclease that cleaves mRNAs containing nonsense codons in metazoan. *RNA* **14,** 2609–2617
17. Eberle, A. B., Lykke-Andersen, S., Mühlemann, O., and Jensen, T. H. (2009) SMG6 promotes endonucleolytic cleavage of nonsense mRNA in human cells. *Nat. Struct. Mol. Biol.* **16,** 49–55
18. Muhlrad, D., and Parker, R. (1994) Premature translational termination

triggers mRNA decapping. *Nature* **370,** 578–581
19. Hoshino, S., Imai, M., Kobayashi, T., Uchida, N., and Katada, T. (1999) The eukaryotic polypeptide chain releasing factor (eRF3/GSPT) carrying the translation termination signal to the 3′-poly(A) tail of mRNA. Direct association of eRF3/GSPT with polyadenylate-binding protein. *J. Biol. Chem.* **274,** 16677–16680
20. Hosoda, N., Kobayashi, T., Uchida, N., Funakoshi, Y., Kikuchi, Y., Hoshino, S., and Katada, T. (2003) Translation termination factor eRF3 mediates mRNA decay through the regulation of deadenylation. *J. Biol. Chem.* **278,** 38287–38291
21. Funakoshi, Y., Doi, Y., Hosoda, N., Uchida, N., Osawa, M., Shimada, I., Tsujimoto, M., Suzuki, T., Katada, T., and Hoshino, S. (2007) Mechanism of mRNA deadenylation: evidence for a molecular interplay between translation termination factor eRF3 and mRNA deadenylases. *Genes Dev.* **21,** 3135–3148
22. van Hoof, A., Frischmeyer, P. A., Dietz, H. C., and Parker, R. (2002) Exosome-mediated recognition and degradation of mRNAs lacking a termination codon. *Science* **295,** 2262–2264
23. Frischmeyer, P. A., van Hoof, A., O'Donnell, K., Guerrerio, A. L., Parker, R., and Dietz, H. C. (2002) An mRNA surveillance mechanism that eliminates transcripts lacking termination codons. *Science* **295,** 2258–2261
24. Kong, J., and Liebhaber, S. A. (2007) A cell type-restricted mRNA surveillance pathway triggered by ribosome extension into the 3′ untranslated region. *Nat. Struct. Mol. Biol.* **14,** 670–676
25. Brown, J. T., Bai, X., Johnson, A. W. (2000) The yeast antiviral proteins Ski2p, Ski3p, and Ski8p exist as a complex *in vivo*. *RNA* **6,** 449–457
26. Lebreton, A., Tomecki, R., Dziembowski, A., and Séraphin, B. (2008) Endonucleolytic RNA cleavage by a eukaryotic exosome. *Nature* **456,** 993–996
27. Doma, M. K., and Parker, R. (2006) Endonucleolytic cleavage of eukaryotic mRNAs with stalls in translation elongation. *Nature* **440,** 561–564
28. Harigaya, Y., and Parker, R. (2010) No-go decay: a quality control mechanism for RNA in translation. *Wiley Interdiscip. Rev. RNA* **1,** 132–141
29. Onouchi, H., Nagami, Y., Haraguchi, Y., Nakamoto, M., Nishimura, Y., Sakurai, R., Nagao, N., Kawasaki, D., Kadokura, Y., and Naito, S. (2005) Nascent peptide-mediated translation elongation arrest coupled with mRNA degradation in the *CGS1* gene of *Arabidopsis*. *Genes Dev.* **19,** 1799–1810
30. Lee, H. H., Kim, Y.-S., Kim, K. H., Heo, I., Kim, S. K., Kim, O., Kim, H. K., Yoon, J. Y., Kim, H. S., Kim, D. J., Lee, S. J., Yoon, H. J., Kim, S. J., Lee, B. G., Song, H. K., Kim, V. N., Park, C. M., and Suh, S. W. (2007) Structural and functional insights into Dom34, a key component of no-go mRNA decay. *Mol. Cell* **27,** 938–950
31. Passos, D. O., Doma, M. K., Shoemaker, C. J., Muhlrad, D., Green, R., Weissman, J., Hollien, J., and Parker, R. (2009) Analysis of Dom34 and its function in no-go decay. *Mol. Biol. Cell* **20,** 3025–3032
32. van den Elzen, A. M. G., Henri, J., Lazar, N., Gas, M. E., Durand, D., Lacroute, F., Nicaise, M., van Tilbeurgh, H., Séraphin, B., and Graille, M. (2010) Dissection of Dom34-Hbs1 reveals independent functions in two RNA quality control pathways. *Nat. Struct. Mol. Biol.* **17,** 1446–1452
33. Becker, T., Armache, J.-P., Jarasch, A., Anger, A. M., Villa, E., Sieber, H., Motaal, B. A., Mielke, T., Berninghausen, O., and Beckmann, R. (2011) Structure of the no-go mRNA decay complex Dom34-Hbs1 bound to a stalled 80S ribosome. *Nat. Struct. Mol. Biol.* **18,** 715–720
34. Shoemaker, C. J., Eyler, D. E., and Green, R. (2010) Dom34:Hbs1 promotes subunit dissociation and peptidyl-tRNA drop-off to initiate no-go decay. *Science* **330,** 369–372
35. Pisareva, V. P., Skabkin, M. A., Hellen, C. U. T., Pestova, T. V., and Pisarev, A. V. (2011) Dissociation by Pelota, Hbs1 and ABCE1 of mammalian vacant 80S ribosomes and stalled elongation complexes. *EMBO J.* **30,** 1804–1817
36. Akimitsu, N., Tanaka, J., and Pelletier, J. (2007) Translation of nonSTOP mRNA is repressed post-initiation in mammalian cells. *EMBO J.* **26,** 2327–2338
37. Chatr-Aryamontri, A., Angelini, M., Garelli, E., Tchernia, G., Ramenghi, U., Dianzani, I., and Loreni, F. (2004) Nonsense-mediated and nonstop decay of ribosomal protein S19 mRNA in Diamond-Blackfan anemia. *Hum. Mutat.* **24,** 526–533
38. Klauer, A. A., and van Hoof, A. (2012) Degradation of mRNAs that lack a stop codon: a decade of nonstop progress. *Wiley Interdiscip. Rev. RNA* **3,** 649–660
39. Torres-Torronteras, J., Rodriguez-Palmero, A., Pinós, T., Accarino, A., Andreu, A. L., Pintos-Morell, G., and Martíí, R. (2011) A novel nonstop mutation in *TYMP* does not induce nonstop mRNA decay in a MNGIE patient with severe neuropathy. *Hum. Mutat.* **32,** E2061–E2068
40. Ruan, L., Osawa, M., Hosoda, N., Imai, S., Machiyama, A., Katada, T., Hoshino, S., and Shimada, I. (2010) Quantitative characterization of Tob interactions provides the thermodynamic basis for translation termination-coupled deadenylase regulation. *J. Biol. Chem.* **285,** 27624–27631
41. Hosoda, N., Funakoshi, Y., Hirasawa, M., Yamagishi, R., Asano, Y., Miyagawa, R., Ogami, K., Tsujimoto, M., and Hoshino, S. (2011) Anti-proliferative protein Tob negatively regulates CPEB3 target by recruiting Caf1 deadenylase. *EMBO J.* **30,** 1311–1323
42. Ito-Harashima, S., Kuroha, K., Tatematsu, T., and Inada, T. (2007) Translation of the poly(A) tail plays crucial roles in nonstop mRNA surveillance via translation repression and protein destabilization by proteasome in yeast. *Genes Dev.* **21,** 519–524
43. Inada, T., and Aiba, H. (2005) Translation of aberrant mRNAs lacking a termination codon or with a shortened 3′-UTR is repressed after initiation in yeast. *EMBO J.* **24,** 1584–1595
44. van Hoof, A. (2005) Conserved functions of yeast genes support the duplication, degeneration and complementation model for gene duplication. *Genetics* **171,** 1455–1461
45. Wilson, M. A., Meaux, S., and van Hoof, A. (2007) A genomic screen in yeast reveals novel aspects of nonstop mRNA metabolism. *Genetics* **177,** 773–784
46. Bengtson, M. H., and Joazeiro, C. A. P. (2010) Role of a ribosome-associated E3 ubiquitin ligase in protein quality control. *Nature* **467,** 470–473
47. Chu, J., Hong, N. A., Masuda, C. A., Jenkins, B. V., Nelms, K. A., Goodnow, C. C., Glynne, R. J., Wu, H., Masliah, E., Joazeiro, C. A. P., and Kay, S. A. (2009) A mouse forward genetics screen identifies LISTERIN as an E3 ubiquitin ligase involved in neurodegeneration. *Proc. Natl. Acad. Sci. U.S.A.* **106,** 2097–2103
48. Hentze, M. W., Caughman, S. W., Casey, J. L., Koeller, D. M., Rouault, T. A., Harford, J. B., and Klausner, R. D. (1988) A model for the structure and functions of iron-responsive elements. *Gene* **72,** 201–208
49. Thermann, R., Neu-Yilik, G., Deters, A., Frede, U., Wehr, K., Hagemeier, C., Hentze, M. W., and Kulozik, A. E. (1998) Binary specification of nonsense codons by splicing and cytoplasmic translation. *EMBO J.* **17,** 3484–3494
50. Anderson, J. S., and Parker, R. (1998) The 3′ to 5′ degradation of yeast mRNAs is a general mechanism for mRNA turnover that requires the SKI2 DEVH box protein and 3′ to 5′ exonucleases of the exosome complex. *EMBO J.* **17,** 1497–1506
51. Wang, L., Lewis, M. S., and Johnson, A. W. (2005) Domain interactions within the Ski2/3/8 complex and between the Ski complex and Ski7p. *RNA* **11,** 1291–1302
52. Schaeffer, D., Tsanova, B., Barbas, A., Reis, F. P., Dastidar, E. G., Sanchez-Rotunno, M., Arraiano, C. M., and van Hoof, A. (2009) The exosome contains domains with specific endoribonuclease, exoribonuclease and cytoplasmic mRNA decay activities. *Nat. Struct. Mol. Biol.* **16,** 56–62
53. Schaeffer, D., and van Hoof, A. (2011) Different nuclease requirements for exosome-mediated degradation of normal and nonstop mRNAs. *Proc. Natl. Acad. Sci. U.S.A.* **108,** 2366–2371
54. Tomecki, R., Kristiansen, M. S., Lykke-Andersen, S., Chlebowski, A., Larsen, K. M., Szczesny, R. J., Drazkowska, K., Pastula, A., Andersen, J. S., Stepien, P. P., Dziembowski, A., and Jensen, T. H. (2010) The human core exosome interacts with differentially localized processive RNases: hDIS3 and hDIS3L. *EMBO J.* **29,** 2342–2357
55. Kobayashi, K., Kikuno, I., Kuroha, K., Saito, K., Ito, K., Ishitani, R., Inada, T., Nureki, O. (2010) Structural basis for mRNA surveillance by archaeal Pelota and GTP-bound EF1α complex. *Proc. Natl. Acad. Sci. U.S.A.* **107,** 17575–17579
56. Chen, L., Muhlrad, D., Hauryliuk, V., Cheng, Z., Lim, M. K., Shyp, V., Parker, R., Song, H. (2010) Structure of the Dom34-Hbs1 complex and implications for no-go decay. *Nat. Struct. Mol. Biol.* **17,** 1233–1240

57. Shoemaker, C. J., and Green, R. (2011) Kinetic analysis reveals the ordered coupling of translation termination and ribosome recycling in yeast. *Proc. Natl. Acad. Sci. U.S.A.* **108,** E1392–E1398
58. Becker, T., Franckenberg, S., Wickles, S., Shoemaker, C. J., Anger, A. M., Armache, J.-P., Sieber, H., Ungewickell, C., Berninghausen, O., Daberkow, I., Karcher, A., Thomm, M., Hopfner, K. P., Green, R., and Beckmann, R. (2012) Structural basis of highly conserved ribosome recycling in eukaryotes and archaea. *Nature* **482,** 501–506
59. Tsuboi, T., Kuroha, K., Kudo, K., Makino, S., Inoue, E., Kashima, I., and Inada, T. (2012) Dom34:Hbs1 plays a general role in quality-control systems by dissociation of a stalled ribosome at the 3′ end of aberrant mRNA. *Mol. Cell* **46,** 518–529

Surg Today (2013) 43:289–292
DOI 10.1007/s00595-012-0462-8

ORIGINAL ARTICLE

A rare point mutation in the Ras oncogene in hepatocellular carcinoma

Akinobu Taketomi · Ken Shirabe · Jun Muto · Shohei Yoshiya · Takashi Motomura · Yohei Mano · Tohru Ikegami · Tomoharu Yoshizumi · Kenji Sugio · Yoshihiko Maehara

Received: 16 May 2011 / Accepted: 17 May 2011 / Published online: 26 December 2012

Abstract
Purpose The Ras gene is one of the oncogenes most frequently detected in human cancers, and codes for three proteins (K-, N-, and H-Ras). The aim of this study was to examine the mutations in codons 12, 13 and 61 of the three Ras genes in cases of human hepatocellular carcinoma (HCC).
Methods Paired samples of HCC and corresponding non-malignant liver tissue were collected from 61 patients who underwent hepatectomy. A dot-blot analysis was used to analyze the products of the polymerase chain reaction (PCR) amplification of codons 12, 13, and 61 of K-, N- and H-Ras for mutations.
Results Only one mutation (K-Ras codon 13; Gly to Asp) was detected among the 61 patients. Interestingly, this patient had a medical history of surgery for both gastric cancer and right lung cancer. No mutations were found in codons 12 and 61 of K-Ras or codons 12, 13 and 61 of the N-Ras and H-Ras genes in any of the HCCs or corresponding non-malignant tissues.
Conclusions These findings indicated that the activation of Ras proto-oncogenes by mutations in codons 12, 13, and 61 does not play a major role in hepatocellular carcinogenesis.

Keywords Ras · Mutation · Hepatocellular carcinoma · Sorafenib

A. Taketomi (✉) · K. Shirabe · J. Muto · S. Yoshiya · T. Motomura · Y. Mano · T. Ikegami · T. Yoshizumi · K. Sugio · Y. Maehara
Department of Surgery and Science, Graduate School of Medical Sciences, Kyushu University, 3-1-1 Maidashi, Higashi-ku, Fukuoka, Japan
e-mail: taketomi@med.hokudai.ac.jp; taketomi@surg2.med.kyushu-u.ac.jp

Abbreviations

Asp	Asparagine
Glu	Glutamate
Gly	Glycine
HCC	Hepatocellular carcinoma
Lys	Lysine
PCR	Polymerase chain reaction
TTP	Time to progression
Val	Valine

Introduction

Hepatocellular carcinoma (HCC) is a global health problem, accounting for more than 80 % of all primary liver cancers, and is one of the most common malignancies worldwide [1]. Most patients with HCC also present with concomitant cirrhosis, which is the major clinical risk factor for hepatic cancer, and results from alcoholism or infection with the hepatitis B or hepatitis C virus. Primary liver malignancies (95 % of which are HCC) are the third and fifth leading causes of cancer death among males and females, respectively, in Japan [2]. Both liver resection and liver transplantation are potentially curative treatments for HCC [3–5]. Although other treatment options, including percutaneous radiofrequency ablation or chemolipiodolization are also available, there is no standard systemic therapy for advanced cases.

Sorafenib (BAY 43-9006, Nexavar) is a novel oral kinase inhibitor that targets multiple tyrosine kinases in vivo and in vitro, and is widely used for HCC [6]. The main targets of sorafenib are the receptor tyrosine kinase pathways which are frequently deregulated in cancer, such as the Ras pathway. The Ras pathway represents a dominant signaling network promoting cell proliferation and

survival. The binding of different growth factors (e.g. epidermal growth factor: EGF) to their receptors (e.g. epidermal growth factor receptor: EGFR) induces the activation of Ras, which in turn activates c-raf, MEK and ERK. Phosphorylated ERK in the nucleus activates transcription factors that regulate the expression of genes involved in cell proliferation and survival.

A phase II trial involving 137 patients with advanced HCC showed that sorafenib induced partial responses in less than 5 % of patients, but the observed median survival of 9.2 months with a median time to progression of 5.5 months was classified as evidence of potential clinical benefit, since the expected median survival of these patients is 6 months [7]. Consequently, a large phase III clinical trial (SHARP) was conducted in 602 patients with advanced HCC. The results showed a 31 % decrease in the risk of death, with a median survival of 10.6 months in the sorafenib arm versus 7.9 months for placebo [8]. In addition, sorafenib showed a significant benefit in terms of the time to progression (TTP) as assessed by independent radiological review, with a median TTP of 5.5 months for the sorafenib and 2.8 months for the placebo arm.

Because Ras is one of the targets of sorafenib, it is important to determine whether mutations in the Ras gene result in the activation of the Ras/MAPK pathway in human HCCs. However, the relationship between Ras mutations and human HCC has not been fully evaluated. The present study was designed to investigate K-, N- and H-Ras (*KRAS, NRAS, HRAS*) somatic mutations in human HCC.

Materials and methods

Patients and tumor samples

Tumor tissue samples were obtained from 61 Japanese patients who underwent surgical resection for HCC during the period between December 1989 and April 1992 in the Department of Surgery and Science, Kyushu University Hospital, Fukuoka, Japan. Surgically resected tissue samples were frozen at −80 °C immediately after resection and were stored until use in this study. Written informed consent was obtained from all patients examined, and the current study was approved by the Kyushu University ethics committee.

DNA preparation and detection of Ras point mutations

High molecular weight DNA was isolated from frozen tumor samples, as described elsewhere [9]. Selective amplification of the Ras gene sequence was done using a PCR technique. The nucleotide sequences of the primers used are listed in Table 1. The PCR was performed at

Table 1 Ras gene primers used in this study

Gene/codon	Length (bp)	Sequence	
KRAS/12, 13	108	Forward	GACTGAATATAAACTTGTGG
		Reverse	CTATTGTTGGATCATATTCG
KRAS/61	128	Forward	TTCCTACAGGAAGCAAGTAG
		Reverse	CACAAAGAAAGCCCTCCCCA
HRAS/12, 13	63	Forward	GACGGAATATAAGCTGGTGG
		Reverse	TGGATGGTCAGCGCACTCTT
HRAS/61	73	Forward	AGACGTGCCTGTTGGACATC
		Reverse	CGCATGTACTGGTCCCGCAT
NRAS/12, 13	109	Forward	GACTGAGTACAAACTGGTGG
		Reverse	CTCTATGGTGGGATCATATT
NRAS/61	103	Forward	GGTGAAACCTGTTTGTTGGA
		Reverse	ATACACAGAGGAAGCCTTCG

bp base pairs

96 °C to denature the DNA (1 min), at 55 °C (*NRAS*), 57 °C (*KRAS*), 62 °C (*HRAS*) to anneal the primer (30 s), and at 72 °C to synthesize DNA (10 s to 1 min) using Taq DNA polymerase for 35–40 cycles in a DNA thermal cycler (Perkin-Elmer-Cetus). Amplified DNA samples were spotted onto nylon membranes (Hybond N+) for the hybridization analysis. All of the DNA isolated from the 61 tumor samples and the corresponding non-malignant liver tissues were screened for activated point mutations in codons 12, 13, and 61 of all three Ras genes using an oligonucleotide specific for the different sequences. The filters were prehybridized for 1 h at 55 °C in solution A (3.0 M tetramethylammonium chloride, 50 mM Tris-HCI, 2 HIMEDTA, 0.1 % SDS, 5× Denhardt's solution, 100 fg/ml denatured herring sperm DNA), and hybridized for 1 h at 55 °C in the same solution with 5 pmol ^{32}P-labeled probe. These filters were washed twice in 0.3 M NaCl, 0.02 M NaH2PO4, 2 mM EDTA and 0.1 % SDS at room temperature for 5 min, and in solution A without Denhardt's solution and herring sperm DNA, once for 5 min at room temperature and twice for 10 min at 60 °C. These filters were then exposed to Kodak XAR5 film. Human cancer cell lines carrying Ras genes mutations were used as positive controls. The colon cancer cell lines: SW620 (*KRAS* codon 12 GTT:Val), LSI80 (*KRAS* codon 12 GAT:Asp), and LOVO (*KRAS* codon 13 GAC:Asp) were obtained from the Japanese Cancer Research Resources Bank, and KMS4 (*KRAS*s codon 12 TGT:Cys) was provided by Dr. Sugio (Institution?).

Results

The age of the 61 patients ranged from 43 to 79 years (average, 64.1 years), and 46 were males and 15 were

females. The positive rate of hepatitis surface B antigen was 12.9 %, and the positive rate of anti-hepatitis C virus antibody was 72.7 %. The mean tumor size was 4.47 cm.

One of the 61 HCCs (1.6 %) carried a point mutation, which was a G to A transition at codon 13 of the *KRAS* gene (Fig. 1). DNA extracted from the corresponding non-malignant liver tissue had the normal codon, suggesting that mutational activation of K-ras was involved in the malignant transformation in this case. This patient was positive for anti-hepatitis C virus antibodies, and was classified to have Child-Pugh A disease. The diameter of this patient's tumor was 12 cm, and the tumor was composed of well to moderately differentiated hepatocellular carcinoma. Interestingly, this patient had undergone surgery for gastric cancer 18 years before and lung cancer 12 years before the surgery for HCC.

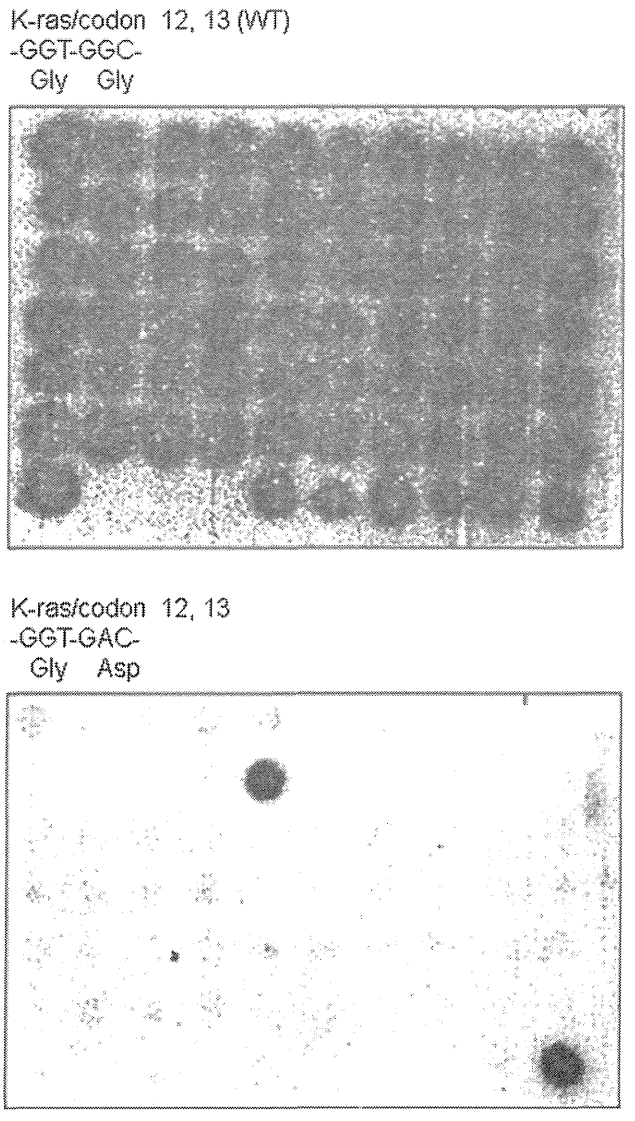

Fig. 1 Detection of a *KRAS* gene mutation in a patient with hepatocellular carcinoma. PCR-amplified DNA from 61 tumor samples was dotted onto nylon membranes and hybridized to a ^{32}P-labeled oligonucleotide probe. *WT* wild type *KRAS*

No mutational activation was found in codons 12 and 61 of *KRAS* or codons 12, 13 and 61 of the *NRAS* and *HRAS* genes in any of the HCCs or corresponding non-malignant tissue samples.

Discussion

This study examined 61 HCC tissues and their corresponding non-malignant liver tissues for a somatic mutation in codons 12, 13, and 61 of the *KRAS*, *HRAS*, or *NRAS* genes, which are known hot spots in various malignancies. However, the study showed the only one of the 61 HCCs (1.6 %) had a somatic mutation in codon 13 of the *KRAS* gene, indicating that Ras gene mutations do not appear to be related to the pathogenesis of most HCCs.

There have been several reports with small sample sizes regarding Ras gene mutations in HCC (Table 2). Most have reported that somatic mutations of the Ras gene in HCCs are uncommon, similar to the current study. Tsuda et al. [10] found only two tumors with Ras point mutations in surgically resected specimens from 30 HCC patients. In their patients, codon 12 of *KRAS* was altered from GGT, coding for Gly, to GTT, coding for Val in one case, and codon 61 of *NRAS* was altered from CAA, coding for Glu, to AAA, coding for Lys, in the other case. Tada et al. analyzed the mutations of the three Ras genes in 23 primary hepatic malignant tumors (12 hepatocellular carcinomas, nine cholangiocarcinomas, and two hepatoblastomas). Point mutations in *KRAS* codon 12 or *KRAS* codon 61 were found in 6 of the 9 cholangiocarcinomas. In contrast, there were no point mutations in any of 12 HCCs or two hepatoblastomas in codons 12, 13, or 61 of the Ras genes. The authors concluded that Ras gene mutations are not related to the pathogenesis of HCC, but play an important role in pathogenesis of cholangiocarcinoma.

Sorafenib is the first molecule with specific targets involved in the pathogenesis of HCC that has become available for routine clinical use. It is an orally applicable

Table 2 Reported Ras gene mutations in HCC patients

Author [references]	No. of patients	Ras gene mutation		
		KRAS	*NRAS*	*HRAS*
Tsuda et al. [10]	30	1 (codon 12)	1 (codon 61)	0
Tada et al. [14]	12	0	0	0
Ogata et al. [15]	19			2
Challen et al. [16]	19	1 (codon 61)	3 (codon 61)	0
Leon et al. [17]	12	1 (codon 61)	0	0
This study	61	1 (codon 13)	0	0

multi-kinase inhibitor that acts by blocking tumor cell proliferation and angiogenesis through the inhibition of serine/threonine kinases [11]. Sorafenib can increase survival by up to 3 months in patients with advanced HCC and acceptable liver function [8]. On the other hand, severe side effects have been reported with sorafenib, including hand-foot skin reactions or liver dysfunction [7, 8]. Therefore, it is important to identify prognostic markers and to establish the proper selection criteria for using sorafenib. Mutations of the Ras genes in cases of HCCs were systemically evaluated in this study because the Ras signaling pathway is the main target of sorafenib. The results indicated that mutational activation of Ras genes is uncommon in the pathogenesis of HCCs. Caraglia et al. [12] reported that the presence of phosphorylated ERK activity in peripheral blood mononuclear cells is valuable for predicting the response to sorafenib therapy in HCC patients. An in vitro study confirmed that phosphorylated ERK was a potential biomarker predicting the sensitivity of HCC to sorafenib [13]. Therefore, a mutation in the RAF/MEK/ERK pathway may be involved in the drug resistance to sorafenib, rather than a Ras mutation.

In summary, only one of 61 HCCs (1.6 %) in the present study carried a point mutation, which was a G to A transition in codon 13 of the *KRAS* gene. No mutational activation was found in codons 12 and 61 of *KRAS* or in codons 12, 13 and 61 of the *NRAS* or *HRAS* genes in any of the HCCs or corresponding non-malignant tissue samples. These findings suggested that Ras gene mutations are not related to the pathogenesis of most HCCs. The signaling pathways downstream of Ras should be examined to identify markers to predict a response to sorafenib.

Acknowledgments We thank Professor Brian Quinn for his review of this manuscript. No financial support was received for this work from any company. This study was supported in part by a grant from the Scientific Research Fund of the Ministry of Education of Japan.

Conflict of interest None of the authors has any conflict of interest.

References

1. El Serag HB, Rudolph KL. Hepatocellular carcinoma: epidemiology and molecular carcinogenesis. Gastroenterology. 2007;132:2557–76.
2. Okita K. Clinical aspects of hepatocellular carcinoma in Japan. Intern Med. 2006;45:229–33.
3. Taketomi A, Kitagawa D, Itoh S, Harimoto N, Yamashita Y, Gion T, et al. Trends in morbidity and mortality after hepatic resection for hepatocellular carcinoma: an institute's experience with 625 patients. J Am Coll Surg. 2007;204:580–7.
4. Taketomi A, Sanefuji K, Soejima Y, Yoshizumi T, Uhciyama H, Ikegami T, et al. Impact of des-gamma-carboxy prothrombin and tumor size on the recurrence of hepatocellular carcinoma after living donor liver transplantation. Transplantation. 2009;87:531–7.
5. Llovet JM, Schwartz M, Mazzaferro V. Resection and liver transplantation for hepatocellular carcinoma. Semin Liver Dis. 2005;25:181–200.
6. Llovet JM, Bruix J. Molecular targeted therapies in hepatocellular carcinoma. Hepatology. 2008;48:1312–27.
7. Abou Alfa GK, Schwartz L, Ricci S, Amadori D, Santoro A, Figer A, et al. Phase II study of sorafenib in patients with advanced hepatocellular carcinoma. J Clin Oncol. 2006;24:4293–300.
8. Llovet JM, Ricci S, Mazzaferro V, Hilgard P, Gane E, Blanc JF, et al. Sorafenib in advanced hepatocellular carcinoma. N Engl J Med. 2008;359:378–90.
9. Sugio K, Ishida T, Yokoyama H, Inoue T, Sugimachi K, Sasazuki T. Ras gene mutations as a prognostic marker in adenocarcinoma of the human lung without lymph node metastasis. Cancer Res. 1992;52:2903–6.
10. Tsuda H, Hirohashi S, Shimosato Y, Ino Y, Yoshida T, Terada M. Low incidence of point mutation of c-Ki-ras and N-ras oncogenes in human hepatocellular carcinoma. Jpn J Cancer Res. 1989;80:196–9.
11. Tanaka S, Arii S. Current status of molecularly targeted therapy for hepatocellular carcinoma: basic science. Int J Clin Oncol. 2010;15:235–41.
12. Caraglia M, Giuberti G, Marra M, Addeo R, Montella L, Murolo M, et al. Oxidative stress and ERK1/2 phosphorylation as predictors of outcome in hepatocellular carcinoma patients treated with sorafenib plus octreotide LAR. Cell Death Dis. 2011;2:e150.
13. Zhang Z, Zhou X, Shen H, Wang D, Wang Y. Phosphorylated ERK is a potential predictor of sensitivity to sorafenib when treating hepatocellular carcinoma: evidence from an in vitro study. BMC Med. 2009;7:41.
14. Tada M, Omata M, Ohto M. Analysis of ras gene mutations in human hepatic malignant tumors by polymerase chain reaction and direct sequencing. Cancer Res. 1990;50:1121–4.
15. Ogata N, Kamimura T, Asakura H. Point mutation, allelic loss and increased methylation of c-Ha-ras gene in human hepatocellular carcinoma. Hepatology. 1991;13:31–7.
16. Challen C, Guo K, Collier JD, Cavanagh D, Bassendine MF. Infrequent point mutations in codons 12 and 61 of ras oncogenes in human hepatocellular carcinomas. J Hepatol. 1992;14:342–6.
17. Leon M, Kew MC. Analysis of ras gene mutations in hepatocellular carcinoma in southern African blacks. Anticancer Res. 1995;15:859–61.

Original Paper

Pathobiology

Pathobiology 2013;80:146–154
DOI: 10.1159/000346196

Received: August 29, 2012
Accepted after revision: November 27, 2012
Published online: January 25, 2013

Tumor-Associated Macrophage Promotes Tumor Progression via STAT3 Signaling in Hepatocellular Carcinoma

Yohei Mano[a, b] Shinichi Aishima[a] Nobuhiro Fujita[c] Yuki Tanaka[a]
Yuichiro Kubo[a] Takashi Motomura[b] Akinobu Taketomi[b] Ken Shirabe[b]
Yoshihiko Maehara[b] Yoshinao Oda[a]

Departments of [a]Anatomic Pathology, [b]Surgery and Science, and [c]Clinical Radiology, Graduate School of Medical Sciences, Kyushu University, Fukuoka, Japan

Key Words
Hepatocellular carcinoma · STAT3 · Macrophage

Abstract
Objective: Signal transducer and activator of transcription 3 (STAT3) is activated in hepatocellular carcinoma (HCC), and tumor-associated macrophage plays an important role in tumor progression. Therefore, we examined STAT3 activation, cytokine expression and infiltration of tumor-associated macrophages in resected HCCs as well as the alteration of cell growth and migration by cytokine stimulation in HCC cell lines. ***Methods:*** Immunohistochemical staining of phosphorylated STAT3 (pSTAT3), CD163, interleukin (IL)-6, Ki-67 and Bcl-XL was performed for 101 cases of resected HCC, and correlations between pSTAT3 staining and clinicopathological findings were analyzed. In HCC cell lines (PLC/PRF/5 and Huh7), cell proliferation and migration by IL-6 stimulation and S3I-201 (STAT3 inhibitor) treatment were analyzed. ***Results:*** In HCC specimens, the pSTAT3-positive group showed high levels of α-fetoprotein ($p = 0.0276$), large tumor size ($p = 0.0092$), frequent intrahepatic metastasis ($p = 0.0214$), high Ki-67 ($p = 0.0002$) and Bcl-XL ($p = 0.0001$), poor prognosis ($p = 0.0234$), and high recurrence rate ($p = 0.0003$). CD163-positive cells were frequently observed in the pSTAT3-positive group ($p = 0.0013$). In two HCC cell lines, IL-6 stimulation promoted cell proliferation and migration via the STAT3 phosphorylation, and S3I-201 inhibited this activation. ***Conclusions:*** STAT3 activation was correlated with aggressive behavior of HCC and may be mediated via tumor-associated macrophage. We expect that STAT3 signaling and tumor-associated macrophages can be attractive therapeutic targets in HCC patients.

Introduction

Hepatocellular carcinoma (HCC) is the fifth most common cause of cancer in the world [1]. Although surgical therapies for HCC have progressed and outcomes of HCC have improved, HCC still often recurs after surgery [2, 3]. Sorafenib, one of the molecular targeted therapies, was reported to show activity against unresectable HCCs;

KARGER

Fax +41 61 306 12 34
E-Mail karger@karger.ch
www.karger.com

1015–2008/13/0803–0146$38.00/0

Accessible online at:
www.karger.com/pat

Yoshinao Oda, PhD
Department of Anatomic Pathology
Graduate School of Medical Sciences, Kyushu University
3-1-1 Maidashi, Higashi-ku, Fukuoka 812-8582 (Japan)
E-Mail oda@surgpath.med.kyushu-u.ac.jp

however, its survival advantage is only 3.7 months [4]. New therapeutic targets are required to improve the survival of patients with HCC.

Signal transducer and activator of transcription 3 (STAT3) is an important molecule in tumor progression [5]. STAT3 activation occurs via phosphorylation and dimerization of tyrosine residue (Tyr705), leading to nuclear entry, DNA binding and gene transcription. STAT3 was regarded as a critical transcription activator for cell cycle- or cell survival-related genes. Bcl-XL is an antiapoptotic protein transcribed by STAT3 activation [6]. Some cytokines such as interleukin (IL)-6 or IL-10 activate STAT3 signaling via their receptors [7]. Constitutive activation of STAT3 has been demonstrated to contribute to tumorigenesis in breast cancer [8], colon cancer [9], lung cancer [10], pancreatic cancer [11], prostate cancer [12], and melanoma [13]. In human HCC, STAT3 phosphorylation was also detected and related to tumor progression [14], angiogenesis [15] and tumorigenesis [16]. The tumor microenvironment is closely associated with the growth of tumor cells, and tumor-associated macrophages play an important role in tumor progression [17]. Macrophages are major inflammatory cells that infiltrate tumors; several studies have shown that high infiltration of tumor-associated macrophages was associated with tumor progression and metastasis [17–20] and predicts poor prognosis in patients with HCC [21]. Tumor-associated macrophages activate STAT3 in ovarian cancer [22] and glioblastoma [23]. However, the correlation between tumor-associated macrophages and STAT3 activation of HCC tumor cells is unknown. Therefore, we examined STAT3 activation, cytokine expression and infiltration of tumor-associated macrophages in resected HCCs and analyzed their association with clinicopathological findings. Alterations in cell growth and migration by cytokine stimulation and STAT3 inhibitor were also analyzed in HCC cell lines.

Materials and Methods

Patients and Samples

One hundred and one available paraffin-embedded specimens from patients with HCC who underwent hepatectomy between January 1997 and December 2001 in our institute were selected by reviewing their pathology data. Any patients undergoing previous or noncurative surgery were excluded. After the surgery, monthly measurement of the serum α-fetoprotein (AFP) level was performed. In addition, ultrasonography and dynamic CT were performed every 3 months. The postoperative survival period or recurrence was entered into the database immediately when a patient died or if recurrence was strongly suspected on diagnostic imaging such as CT or magnetic resonance imaging.

This study conformed to the ethical guidelines of the 1975 Declaration of Helsinki and was approved by the ethics committees of Kyushu University Hospital (grant No. 21-117). Informed consent was obtained from each patient included in the study.

Immunohistochemistry

Sections of resected specimens were fixed in 10% buffered formalin, embedded in paraffin and stained by Envision+ system and DAB kit (Dako, Glostrup, Denmark). Immunohistochemical stains were performed with antibodies of phosphorylated STAT3 (pSTAT3; Tyr 705; D3A7, 1:50; Cell Signaling Technology), CD163 (10D6, 1:200; Novocastra), IL-6 (rabbit polyclonal, 1:1,000; Abcam), Ki-67 (MIB-1, 1:200; Dako), and Bcl-XL (rabbit polyclonal, 1:200; Santa Cruz Biotechnology, Santa Cruz, Calif., US). Sections were pretreated before being incubated with primary antibodies in a microwave oven at 99°C for 20 min for pSTAT3, CD163, IL-6 and Bcl-XL or in a pressure cooker for 25 min for Ki-67.

Each slide was stained in serial sections and examined by two pathologists (Y.M. and S.A.). In nuclear staining of pSTAT3 and Ki-67 and in cytoplasm staining of Bcl-XL, the percent positive cells was estimated by count of 1,000 tumor cells in most staining areas (hot spots). Staining of CD163, a marker of tumor-associated macrophages [19, 22–25], and IL-6 was evaluated by estimating the total counts of cytoplasm or membrane at 3 high-power fields. The mean of nuclear pSTAT3-positive cells in HCCs was 10.7% (range 0–82.0), and pSTAT3 stain was classified into a positive (≥10.7% of tumor cell nuclei) and a negative group (<10.7% of tumor nuclei). Furthermore, in the cases of the pSTAT3-positive group (n = 36), the CD163-positive cells were counted separately in areas of pSTAT3-positive and pSTAT3-negative HCC cells.

For double staining of IL-6 and CD163, HCC specimens were boiled in 10 mM citrate buffer (pH 6.0) for 20 min and incubated with IL-6 primary antibody (1:1,000) at room temperature for 15 min. The sections were washed three times and incubated with anti-rabbit horseradish peroxidase-conjugated polymer at room temperature for 45 min; IL-6 was visualized by DAB kit. Next, the sections were boiled in 10 mM citrate buffer (pH 6.0) for 10 min, incubated with CD163 primary antibody (1:200) for 90 min and incubated with anti-mouse alkaline phosphatase-conjugated polymer at room temperature for 45 min. CD163 of the sections was visualized by New Fuchsin Substrate kit (Nichirei, Tokyo, Japan).

Cell Culture

Human HCC cell lines PLC/PRF/5 and Huh7 were obtained from Riken Bioresource Center, Tsukuba, Japan, and cultured in Dulbecco's modified Eagle's medium (DMEM) supplemented with 1 or 10% fetal bovine serum (FBS). PLC/PRF/5 and Huh7 cells were maintained in DMEM containing 1% FBS for 24 h prior to IL-6 (Peprotech, Rocky Hill, N.J., USA) stimulation. All in vitro experiments were done in triplicate.

Immunoblotting

Cellular proteins were solubilized in lysis buffer containing protease inhibitor and phosphatase inhibitor 30 min after stimulation with IL-6 (20 μg/ml). Equal amounts of protein were separated by SDS-PAGE and then transferred to the polyvinylidene fluoride membrane. Following blocking in Tris buffer containing 2% BSA, the membrane was stained with 1:1,000 dilution of anti-STAT3 (Cell Signaling Technology, Danvers, Mass., USA) and anti-pSTAT3 (Cell Signaling Technology) antibodies, then

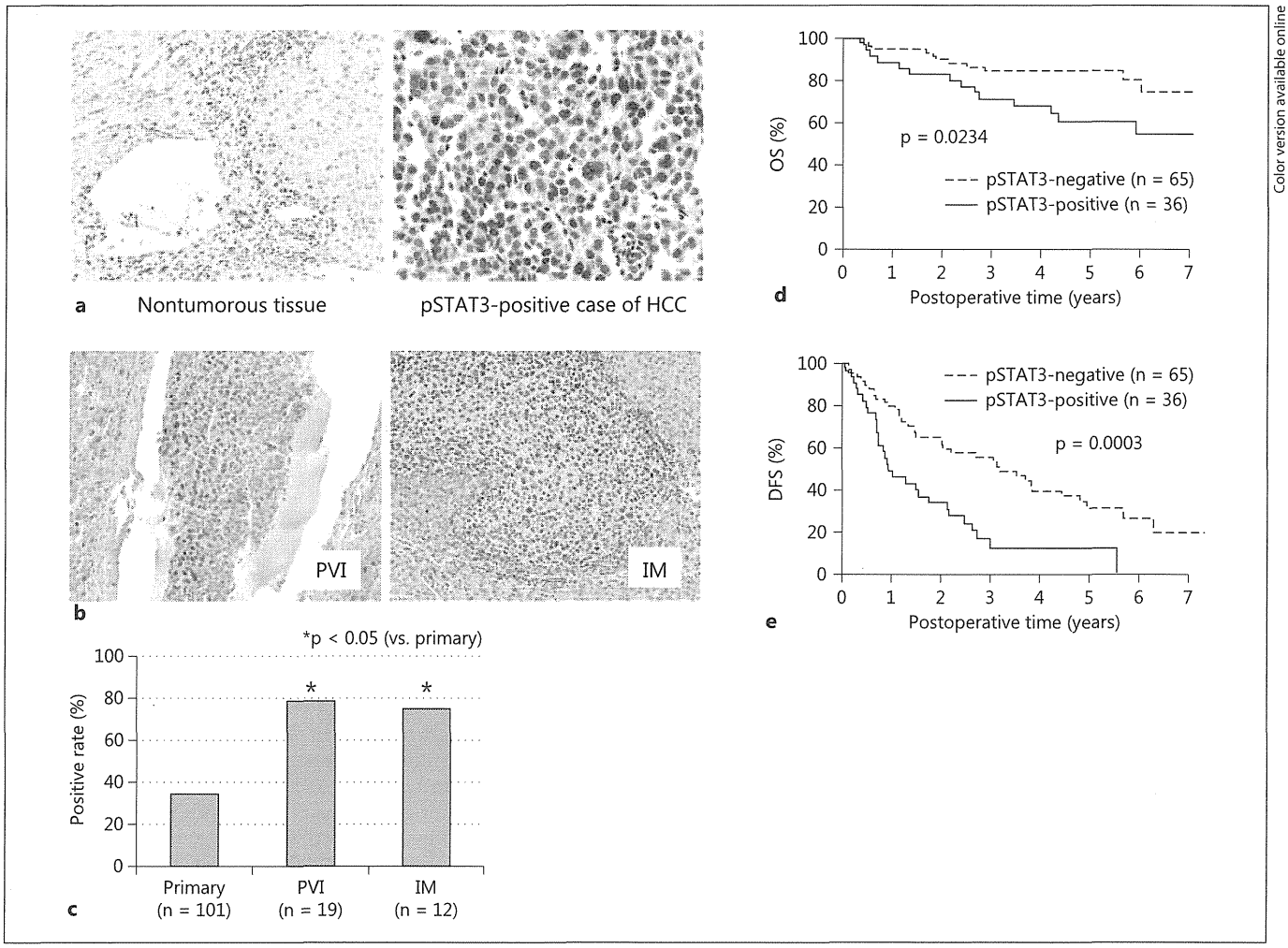

Fig. 1. Immunohistochemical staining of pSTAT3 in HCC. **a** pSTAT3 was expressed in the nucleus. In nontumorous tissue, endothelial cells, bile duct epithelial cells and inflammatory cells were stained by pSTAT3 (left panel). ×100. HCC cells were also stained (82.2%, right panel). ×100. **b** Tumor cells of PVI and IM stained by pSTAT3. ×200. **c** Comparison of pSTAT3 staining in primary HCC, tumor cells of PVI and IM. pSTAT3 staining was significantly prominent in tumor cells of PVI and IM compared with primary HCC ($p < 0.05$). **d**, **e** pSTAT3 expression correlated with poor prognosis. OS (**d**) and DFS (**e**) curves for pSTAT3-positive and pSTAT3-negative groups in patients with HCC (**d**, $p = 0.0234$; **e**, $p = 0.0003$; log-rank test).

washed and incubated with horseradish peroxidase-conjugated secondary antibody (Cell Signaling Technology). Bands were visualized by the enhanced chemiluminescence system (GE Healthcare, UK).

Cell Growth Assay

PLC/PRF/5 and Huh7 cells were seeded at a density of 5×10^4 cells/24-well plates and maintained in conditioned medium for 24 h before stimulation. Viable cells were counted by trypan blue stain 48 h after stimulation with IL-6 (25 ng/ml).

Wound-Healing Assay

PLC/PRF/5 and Huh7 cells were seeded at a density of 5×10^4 cells/6-well plates. Approximately 24 h later, when the cells were 100% confluent, a sterile 100-μl pipette tip was used to longitudinally scratch a constant-diameter strip in the confluent monolayer. The medium and cell debris were aspirated away and replaced by 2 ml of fresh DMEM containing 1% FBS with or without IL-6 (25 ng/ml). Photographs were taken at 0 and 48 h after wounding by phase-contrast microscopy. For statistical analysis, three randomly selected points along each wound were marked, and the horizontal distance between the migrating cells and the initial wound was measured 48 h later.

Inhibition of STAT3

In both cell growth and wound-healing assays, PLC/PRF/5 and Huh7 cells were cultured in DMEM containing 1% FBS and IL-6 (25 ng/ml) with or without 100 nM S3I-201 (NSC 74859; Santa Cruz Biotechnology). S3I-201 was treated 30 min before IL-6 stimulation. DMSO was used for control.

Table 1. Comparison of pSTAT3 expression and clinicopathological findings

pSTAT3 expression	pSTAT3 negative (n = 65)	pSTAT3 positive (n = 36)	p value
Clinical features			
Sex, male/female	55/10	26/10	0.0849
Age, years	63.9±7.3	63.6±9.5	0.8726
HBsAg, +/–	14/51	8/28	0.9922
HCV Ab, +/–	42/23	23/13	0.9798
Cirrhosis	22/43	14/22	0.4990
AFP, ng/ml	852.4±308†	20,673.4±11,688†	0.0276*
DCP, mAU/ml	2,798.2±1,179.1†	6,278.4±3,184.7†	0.2217
Pathological features			
Tumor size, cm	3.7±2.2	5.1±3.2	0.0092*
Differentiation, poor/well and moderate	19/46	16/20	0.1253
Capsule formation	41/24	26/10	0.4619
Infiltration to the capsule	33/32	23/13	0.1681
Portal venous invasion, +/–	30/35	24/12	0.0687
Hepatic venous invasion, +/–	15/50	12/24	0.3031
Intrahepatic metastasis, +/–	18/47	18/18	0.0214*
MIB-1 LI, %	3.5±0.5	10.2±2.2	0.0002*
Bcl-XL, %	13.0±1.5	25.2±2.0	0.0001*

HBsAg = Hepatitis B surface antigen; HCV Ab = hepatitis C virus antibody; DCP = des-γ-carboxy prothorombin. * $p < 0.05$.

Statistical Analysis

Statistical analysis was carried out using Microsoft Excel software and JMP software (SAS Institute, Cary, N.C., USA). Comparison between pSTAT3 staining and clinicopathological findings or staining of other antibodies was evaluated by Pearson's χ^2, Fisher's exact tests and the Mann-Whitney U test. Patient survival analysis including overall survival (OS) and disease-free survival (DFS) was calculated by the Kaplan-Meier method; differences were evaluated by the log-rank test. For multivariate analysis, the Cox proportional hazard model was used. Two-sided Student's t test was applied for analysis of in vitro data. Statistical analyses were considered significant at a p value <0.05.

Results

pSTAT3 Expression in Clinical Samples

pSTAT3 was stained in the nuclei of HCC cells, normal endothelial cells, some bile duct epithelial cells and inflammatory cells. pSTAT3 nuclear staining in HCC cells is displayed in figure 1a. The mean percentage of nuclear pSTAT3-positive cells in HCCs was 10.7% (range 0–82.0). The number of pSTAT3-positive and pSTAT3-negative samples was 36 and 65, respectively. We also examined pSTAT3 staining at the lesions of 19 portal venous invasions (PVIs) and 12 intrahepatic metastases (IMs) in 101 cases. Fifteen of 19 PVIs (78.9%) and 9 of 12 (75.0%) IMs were defined as pSTAT3-positive cases (fig. 1b). Positive rates in both lesions were significantly higher than those in the primary lesions (35.6%; $p < 0.05$; fig. 1c).

Comparison of pSTAT3 Expression and Clinicopathological Findings

A comparison of clinicopathological findings in pSTAT3-positive and pSTAT3-negative groups is summarized in table 1. The pSTAT3-positive group showed higher AFP ($p = 0.0276$), larger tumor size ($p = 0.0092$), more frequent IMs ($p = 0.0214$), a higher Ki-67 labeling index (LI; $p = 0.0002$), and more Bcl-XL-positive cells ($p = 0.0001$) than the pSTAT3-negative group, whereas no significant differences were noted with respect to sex, age, infection of hepatitis viruses, liver cirrhosis, PIVKA II (proteins induced by vitamin K absence or antagonist II), histological differentiation, capsule formation, infiltration to the capsule, and vessel invasion.

Survival Analysis after Surgery

The median follow-up period was 1,391 days (range 36–3,289). pSTAT3 expression was significantly correlated with OS and DFS ($p = 0.0234$ and 0.0003, respectively; fig. 1d, e). Univariate analyses indicated that high AFP (>100 ng/ml), large tumor size (>5 cm), PVIs and IMs were prognostic factors for OS and male sex, hepatitis C virus infection, high AFP (>100 ng/ml) and IMs for DFS (table 2). Multivariate proportional hazard models revealed that high AFP and IMs were independent prognostic factors for OS and pSTAT3 expression and high AFP for DFS (table 2).

Tumor-Associated Macrophage Localization and pSTAT3 Expression of HCCs

CD163-positive cells were localized around the pSTAT3-positive HCC cells (fig. 2a). Figure 2b shows the boxplots of CD163-positive cells (mean ± SD: pSTAT3-negative group, 28.5 ± 15.4; pSTAT3-positive group, 42.6 ± 26.6). The pSTAT3-positive group (n = 36) showed statistically higher CD163-positive cells ($p = 0.0013$; fig. 2b) than the pSTAT3-negative group (n = 65). Furthermore, we analyzed the localization of CD163-posi-

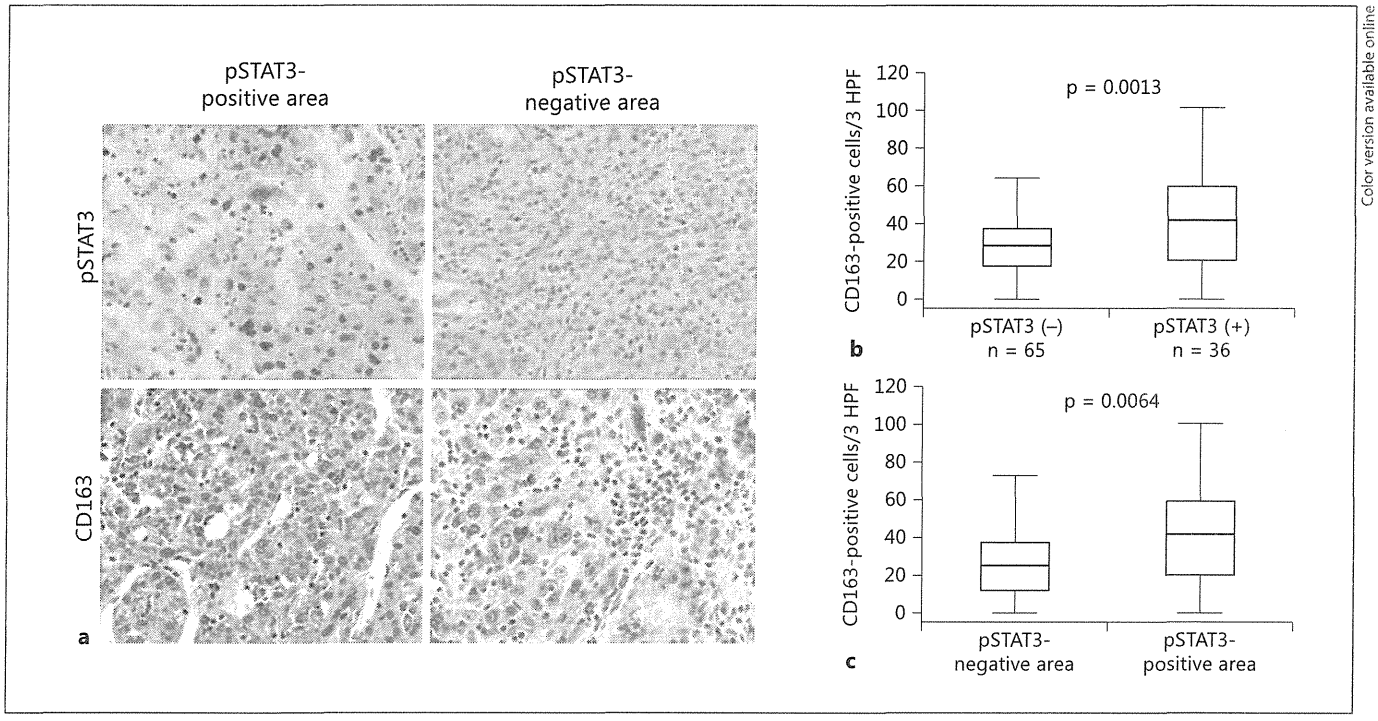

Fig. 2. Tumor-associated macrophages correlated with pSTAT3 expression in HCC. **a** Immunohistochemical staining of pSTAT3 and CD163 in the pSTAT3-positive and pSTAT3-negative area. ×200. **b** Counts of CD163-positive cells between pSTAT3-positve and pSTAT3-negative groups. **c** Counts of CD163-positive cells in areas of pSTAT3-positive and pSTAT3-negative HCC cells existed in the pSTAT3-positive group. HPF = High-power field.

Table 2. Survival analysis after surgery

Variable	Univariate analysis of OS	Multivariate analysis of OS		
	p value	hazard ratio	95% CI	p value
pSTAT3 positive	0.0234*	1.104	0.465–2.683	0.8236
AFP >100 ng/ml	0.0005*	2.968	1.294–7.026	0.0103*
Tumor size >5 cm	0.0246*	1.489	0.610–3.578	0.3755
Portal venous invasion	0.0422*	1.568	0.629–4.1265	0.3367
Intrahepatic metastasis	0.0022*	2.668	1.186–6.194	0.0177*
Variable	Univariate analysis of DFS	Multivariate analysis of DFS		
	p value	hazard ratio	95% CI	p value
pSTAT3 positive	0.0003*	1.851	1.066–3.201	0.0288*
Sex, male	0.0267*	0.978	0.515–1.790	0.9431
HCV Ab (+)	0.0158*	1.672	0.948–3.096	0.0767
AFP >100 ng/ml	0.0002*	2.070	1.218–3.476	0.0076*
Intrahepatic metastasis	0.0012*	1.702	0.964–3.012	0.0664

CI = Confidence interval; HCV Ab = hepatitis C virus antibody. * $p < 0.05$.